AGU PUBLICATIONS

Water Resources Research

RESEARCH ARTICLE
10.1002/2014WR016547

Key Points:
- The DHD scheme gives accurate and stable results in rainfall-runoff computations
- The DHD scheme is almost as simple to code as diffusive wave models
- The DHD scheme avoids the numerical inconveniences of diffusive wave models

Supporting Information:
- Supporting Information S1

Correspondence to:
L. Cea,
luis.cea@udc.es

Citation:
Cea, L., and E. Bladé (2015), A simple and efficient unstructured finite volume scheme for solving the shallow water equations in overland flow applications, *Water Resour. Res.*, *51*, 5464–5486, doi:10.1002/2014WR016547.

Received 12 OCT 2014
Accepted 1 JUN 2015
Accepted article online 6 JUN 2015
Published online 19 JUL 2015

A simple and efficient unstructured finite volume scheme for solving the shallow water equations in overland flow applications

L. Cea[1] and E. Bladé[2]

[1]Environmental and Water Engineering Group, Departamento de Métodos Matemáticos y de Representación, Universidade da Coruña, A Coruña, Spain, [2]Institut FLUMEN, E.T.S. d'Eng. De Camins, Canals i Ports de Barcelona, Universitat Politécnica de Catalunya, Barcelona, Spain

Abstract This paper presents the decoupled hydrological discretization (DHD) scheme for solving the shallow water equations in hydrological applications involving surface runoff in rural and urban basins. The name of the scheme is motivated by the fact that the three equations which form the two-dimensional shallow water system are discretized independently from each other and thus, the numerical scheme is decoupled in a mathematical sense. Its main advantages compared to other classic finite volume schemes for the shallow water equations are its simplicity to code and the lower computational cost per time step. The validation of the scheme is presented in five test cases involving overland flow and rainfall-runoff transformation over topographies of different complexity. The scheme is compared to the finite volume scheme of Roe (1986), to the simple inertia formulation, and to the diffusive wave model. The test cases show that the DHD scheme is able to compute subcritical and supercritical flows in rural and urban environments, and that in overland flow applications it gives similar results to the second-order scheme of Roe with a lower computational cost. The results obtained with the simple inertia and diffusive wave models are very similar to those obtained with the DHD scheme in rural basins in which the bed friction and topography dominate the flow hydrodynamics but they deteriorate in typical urban configurations in which the presence of supercritical flow conditions and small-scale patterns boost the relevance of the inertial terms in the momentum equations.

1. Introduction

Two-dimensional shallow water models (also known as dynamic wave models) are increasingly used in the computation of overland flow and rainfall-runoff transformation in urban and meso-scale rural basins [*Cea et al.*, 2010b; *Costabile et al.*, 2012; *Howes et al.*, 2006; *Hunter et al.*, 2007, 2008; *Kivva and Zheleznyak*, 2005; *Sanders et al.*, 2008; *Schubert et al.*, 2008]. Although kinematic and diffusive wave models have been traditionally preferred for these applications due to their lower computational cost when applied at the catchment scale, it has been recognized that the diffusive wave (DW) equation presents a series of inconveniences in comparison to the dynamic wave equation due to the fact of neglecting the inertial terms in the momentum balance [*Bates et al.*, 2010; *Costabile et al.*, 2012]. Dimensional analysis shows that the relative importance of the inertial terms increases with the Froude number and with the small-scale features of the flow [*Hunter et al.*, 2007]. Therefore, the results given by DW models deteriorate in supercritical flow conditions or when the spatial gradients of velocity become important. A second problem related to explicit implementations of the DW approximation is that the maximum stable time step decreases with the square of the mesh size, while it decreases linearly in the case of the shallow water equations. This increases greatly the computational requirements when the DW model is used in combination with high-resolution grids. The previous problems are more relevant in urban basins, where supercritical conditions are quite common and the mesh size and length scales are usually smaller than in rural catchments. On the other hand, the main advantage of DW models is their computational efficiency when used with coarse meshes and the simplicity of the numerical schemes used to solve the equations. DW models and other simplified versions of the shallow water equations might therefore be advantageous in large-scale problems dominated by bed friction and topography [*Hunter et al.*, 2007], in which the role of the inertial terms is negligible. However, in order to achieve a high-computational efficiency with a DW model it is necessary to

implement flow limiters which depend on nonphysical parameters and which make the velocity and water depth results more sensitive to the grid size and time step than to bed friction [*Bates et al*., 2010; *Hunter et al*., 2005].

The availability of high-resolution DTM's, the increasing computing power and the development of parallelization techniques [*Neal et al*., 2010; *Sanders et al*., 2010], are making possible the computation of rainfall-runoff transformation in rural basins of several km^2 with very fine numerical meshes, which promotes the resolution of small-scale flow patterns and therefore, increases the relevance of inertial terms in the solution. As the spatial resolution of the numerical discretizations and DTM's increases, the use of inertial formulations at the basin and hillslope scales becomes more advantageous. The results presented in *Bates et al*. [2010] show that even with mesh resolutions of 50 m, depending on the topography and bed roughness it might be advantageous to use an inertial formulation rather than a purely diffusive model.

Shallow water models do not have any of the previous inconveniences since they retain all the inertial terms in the momentum equations, but their performance in terms of numerical stability and computational cost in rainfall-runoff applications depends strongly on the numerical scheme used to solve them. The scheme must be accurate and robust to avoid instabilities in the solution due to the presence of highly unsteady wet-dry fronts with water depths of a few millimeters over very rough, complex, and steep terrains. At the same time, the numerical discretization must ensure the conservation of water mass in order to compute properly the shape of the outlet hydrograph. In this context, finite volume schemes are very popular for solving the shallow water equations because they ensure mass conservation in the whole system as long as an appropriate treatment of the wet-dry fronts is used. The finite volume discretization of the advective terms in the shallow water equations has been the purpose of many publications over the last 30 years (for a review the reader is referred to *Canestrelli et al*. [2009], *LeVeque* [2002], and *Toro* [2001, 2009, and references therein]). Several works have shown that, when applied to complex and rough terrains, and more specifically to overland flow modeling, these schemes need to be complemented with an appropriate discretization of the topography, wet-dry fronts and bed friction in order to avoid instabilities in the solution and to improve model accuracy [*Bermúdez et al*., 1998; *Bradford and Sanders*, 2002; *Cea and Vázquez-Cendón*, 2012; *Delestre and Marche*, 2011; *Kim et al*., 2008; *Liang*, 2010; *Ricchiuto et al*., 2007, 2011; *Vázquez-Cendón*, 1999]. These discretization schemes for the advective terms and topography give rise to complex implementations and expensive numerical solutions which, in addition, condition the numerical discretization used in sediment and solute transport equations linked to the shallow water model [*Audusse and Bristeau*, 2003; *Benkhaldoun et al*., 2007; *Cea and Vázquez-Cendón*, 2012; *Murillo et al*., 2008]. The use of these kind of discretization techniques is very convenient in applications involving shock waves but, as it will shown in the test cases presented in this paper, they are not strictly necessary for overland flow applications.

The purpose of this paper is to present, validate, and evaluate a simple and computationally efficient numerical scheme for solving the two-dimensional shallow water equations in hydrological applications involving overland flow and rainfall-runoff transformation. Such a discretization can be applied to solve in a unified way overland flow and inundation flow at the basin and at the reach scales, without the need of using two separate models. The main advantages of the proposed discretization compared to other classic finite volume schemes for the shallow water equations are its simplicity to code and the lower computational cost per time step. The proposed scheme is validated with laboratory and field experimental data in five different test cases involving flow conditions typical from urban and rural basins, and length scales ranging from 1 m to several km. The two first test cases are representative of urban basins, with a low bed roughness, transcritical flow conditions and a relatively fine numerical grid. The third and forth test cases involve rainfall-runoff transformation in rural watersheds of a few km^2 with high bed friction coefficients, Froude numbers lower than one and relatively coarse computational grids. Lastly, a dam break test case is presented to show the performance of the scheme under the presence of unsteady strong shock waves.

The scheme is compared in terms of computational time, numerical stability, and accuracy to the classic finite volume scheme of *Roe* [1986], to the simple inertia (SI) formulation [*Bates et al*., 2010; *de Almeida et al*., 2012; *Ponce*, 1990] and to a DW model. As demonstrated in *de Almeida and Bates* [2013], the SI formulation and the DW equations are not suitable to model supercritical flow conditions and therefore, the comparison with those models is not presented in all the test cases. All the schemes have been implemented in the shallow water model Iber [*Bladé et al*., 2014], which was used in all the computations presented in this paper.

2. Numerical Discretization

2.1. The Decoupled Hydrological Discretization (DHD) Scheme for the Shallow Water Equations

Hydrological models based on the 2-D shallow water equations solve the following set of mass and momentum conservation equations:

$$\begin{aligned}
&\frac{\partial h}{\partial t}+\frac{\partial q_x}{\partial x}+\frac{\partial q_y}{\partial y}=R-f\\
&\frac{\partial q_x}{\partial t}+\frac{\partial}{\partial x}\left(\frac{q_x^2}{h}+\frac{gh^2}{2}\right)+\frac{\partial}{\partial y}\left(\frac{q_x q_y}{h}\right)=-gh\frac{\partial z_b}{\partial x}-g\frac{n^2}{h^{7/3}}|\mathbf{q}|q_x\\
&\frac{\partial q_y}{\partial t}+\frac{\partial}{\partial x}\left(\frac{q_x q_y}{h}\right)+\frac{\partial}{\partial y}\left(\frac{q_y^2}{h}+\frac{gh^2}{2}\right)=-gh\frac{\partial z_b}{\partial y}-g\frac{n^2}{h^{7/3}}|\mathbf{q}|q_y
\end{aligned} \tag{1}$$

where z_b is the bed elevation, (q_x, q_y) are the two components of the unit discharge, $|\mathbf{q}|$ is the modulus of the unit discharge, h is the water depth, n is the Manning coefficient, g is the gravity acceleration, R is the rainfall intensity, and f represents the rainfall losses, which might be due to infiltration, evapotranspiration, interception, and surface detention. Although Manning formula has been used in equation (1) to model bed friction, other formulations as Keulegan, Chezy, or Darcy are possible, and do not affect the analysis and results presented in this paper.

Equations (1) can be rewritten as:

$$\begin{aligned}
&\frac{\partial h}{\partial t}+\frac{\partial q_x}{\partial x}+\frac{\partial q_y}{\partial y}=R-f\\
&\frac{\partial q_x}{\partial t}+\frac{\partial}{\partial x}\left(\frac{q_x^2}{h}\right)+\frac{\partial}{\partial y}\left(\frac{q_x q_y}{h}\right)=-gh\frac{\partial z_s}{\partial x}-gh\frac{n^2|\mathbf{q}|}{h^{10/3}}q_x\\
&\frac{\partial q_y}{\partial t}+\frac{\partial}{\partial x}\left(\frac{q_x q_y}{h}\right)+\frac{\partial}{\partial y}\left(\frac{q_y^2}{h}\right)=-gh\frac{\partial z_s}{\partial y}-gh\frac{n^2|\mathbf{q}|}{h^{10/3}}q_y
\end{aligned} \tag{2}$$

where $z_s = z_b + h$ is the free surface elevation. The only difference between equations (1) and (2) is that in (1) the hydrostatic pressure gradient is included in the same term as the flux of inertia, while in (2) it is merged with the bed slope in a single term involving the free surface gradient. The advantage of using equations (2) as the basis for a discretization scheme is that an exact balance between the hydrostatic pressure gradient and the bed slope is obtained naturally when the free surface is horizontal, since both of them are merged in a single term. If equations (1) are used, a special upwind discretization of the bed slope is needed to achieve this balance [*Bermúdez and Vázquez-Cendón*, 1994]. The upwind discretization of the bed slope has been the purpose of many research efforts in the last years, and it has led to complex upwind discretizations in order to obtain well-balanced schemes which preserve the hydrostatic solution [*Bermúdez and Vázquez-Cendón*, 1994; *Canestrelli et al*., 2009; *Cea and Vázquez-Cendón*, 2012; *Kim et al*., 2008; *Liang*, 2010; *Liang and Marche*, 2009]. On the other hand, the advantage of using equations (1) is that the hydrostatic pressure gradient is a momentum flux and therefore, it seems sensible to discretize it together with the flux of inertia in a single momentum flux term. In problems involving shock waves, the momentum balance between advective inertia and hydrostatic pressure is vital in order to correctly reproduce the location of the hydraulic jump. In those situations a discretization based on equations (1) should be more convenient.

The majority of the numerical schemes developed for the shallow water equations have been applied to the equations written as in (1) [*Begnudelli et al*., 2008; *Berthon et al*., 2011; *Canestrelli et al*., 2009; *Cea and Vázquez-Cendón*, 2012; *Chertock et al*., 2010; *LeVeque*, 2002; *Liang*, 2010; *Martinez-Gavara and Donat*, 2011; *Sanders et al*., 2008; *Toro*, 2001; *Wang et al*., 2011]. There are however some discretization schemes which have been applied to the shallow water equations written as in (2), although they are less frequent in the scientific literature [*Duan*, 2004; *Liang et al*., 2007; *Sauvaget et al*., 2000; *Wu*, 2004]. We will use the form (2) for the DHD scheme presented here.

In the following, the discretization scheme will be applied to an unstructured collocated finite volume mesh formed by control volumes (or cells) of any number of faces, but it might be equally applied to structured grids. Figure 1 shows a sketch of two neighbor cells and the geometric variables which will be used in the

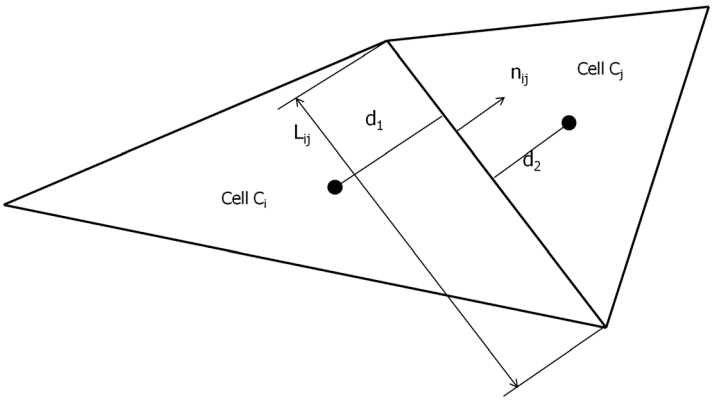

Figure 1. Sketch of the unstructured finite-volume discretization used in the solver, showing the geometric variables used to compute the flux between the cells C_i and C_j.

discretization. All the flow variables (water depth, unit discharge, bed elevation, free surface elevation) are stored at the geometric center of the control volumes. The mass and momentum conservation equations are discretized independently, thus, the model is decoupled in a mathematical sense, which motivates the name of the scheme. Since the discretization of the momentum conservation equations in the x and y directions is analogous, only the x momentum equation will be considered in the following.

Equations (2) are integrated in time using an explicit Euler scheme, and in space over a control volume C_i using Gauss theorem, to obtain:

$$\frac{h_i^{n+1}-h_i^n}{\Delta t}A_i+\sum_{j\in K_i}Q_{ij}^n=\left(R_i^n-f_i^n\right)A_i \tag{3}$$

$$\frac{q_{x,i}^{n+1}-q_{x,i}^n}{\Delta t}A_i+\sum_{j\in K_i}F_{x,ij}^n=\left(T_{x,i}^{n+1}-gh_i^nS_{x,i}^n\right)A_i \tag{4}$$

where K_i accounts for all the control volumes C_j which share any face with C_i, A_i is the area of the control volume C_i, Q_{ij}, and $F_{x,ij}$ are, respectively, the numerical approximations of the fluxes of mass and inertia in the x direction between the adjacent control volumes C_i and C_j, and R_i, f_i, $S_{x,I}$, and $T_{x,i}$ are, respectively, centered discretizations of the rainfall intensity, rainfall losses, free surface gradient in the x direction and bed friction stress in the x direction. The superindexes n and $n+1$ indicate the time step at which each term is evaluated. The discretization given by equation (3) is mass conservative since at each time step the flux of mass (Q_{ij}) leaving one control volume by one of its faces is exactly the same as the discharge entering the adjacent cell, which guarantees the global conservation of mass in the whole numerical grid.

The numerical approximation of the mass and momentum fluxes (Q_{ij} and $F_{x,ij}$) can be computed using a simple upwind scheme as:

$$Q_{ij}=\lambda_{ij}h_{ij}^UL_{ij}\qquad F_{x,ij}=\lambda_{ij}q_{x,ij}^UL_{ij}\qquad \lambda_{ij}=U_{x,ij}n_{x,ij}+U_{y,ij}n_{y,ij} \tag{5}$$

$$h_{ij}^U=\begin{cases}h_i & \text{if } \lambda_{ij}\geq 0\\ h_j & \text{if } \lambda_{ij}<0\end{cases}\qquad q_{x,ij}^U=\begin{cases}q_{x,i} & \text{if } \lambda_{ij}\geq 0\\ q_{x,j} & \text{if } \lambda_{ij}<0\end{cases} \tag{6}$$

where L_{ij} is the length of the cell face which joins the control volumes C_i and C_j, $(U_{x,ij}, U_{y,ij})$ are the two components of the velocity at the cell face, $(n_{x,ij}, n_{y,ij})$ are the two components of the unit normal vector to the cell face, and λ_{ij} is the velocity component normal to the cell face. The velocity components at the cell face are computed from linear interpolation between the control volume centroids as $U_{x,ij}=U_{x,i}\alpha_{ij}+U_{x,j}(1-\alpha_{ij})$, with an analogous expression for $U_{y,ij}$. The linear interpolation coefficient is computed as $\alpha_{ij}=d_2/(d_1+d_2)$, where the distances d_1 and d_2 are defined in Figure 1. In equations (5) and (6), it has been assumed without loss of generality that the unit normal vector points from the cell C_i to the cell C_j (Figure 1) and therefore, λ_{ij} is positive if the flow goes from C_i to C_j and negative otherwise.

Using the upwind definition of the mass flux Q_{ij} given by equation (5) leads to numerical instabilities as the water velocity tends to zero. This is because the numerical diffusion of the discretization defined by equation (5) is proportional to the water velocity and it does not depend on the celerity of the free surface gravity waves ($c=\sqrt{gh}$). This is undesirable in problems in which the surface runoff accumulates in the presence of terrain depressions, forming ponds where the velocity tends to zero. In order to improve the numerical

stability of the scheme and to preclude the development of nonphysical oscillations, the definition of the mass flux Q_{ij} given by equation (5) is corrected with a term which depends on the celerity of gravity waves and on the difference of the water surface elevation and depth across the cell face as:

$$Q_{ij} = \lambda_{ij} h_{ij}^{U} L_{ij} - 0.5\sqrt{g h_{ij}}\,\Delta_{ij} L_{ij} \tag{7}$$

$$\Delta_{ij} = \begin{cases} \max\left[0,\ \min\left(z_{s,j} - z_{s,i},\ h_j - h_i\right)\right] & \text{if } z_{s,j} - z_{s,i} \geq 0 \\ \min\left[0,\ \max\left(z_{s,j} - z_{s,i},\ h_j - h_i\right)\right] & \text{if } z_{s,j} - z_{s,i} < 0 \end{cases} \tag{8}$$

where Δ_{ij} shifts between the free surface elevation difference and the water depth difference across the cell face, by means of a Minmod type limiter. The correction term is only introduced when the surface elevation at both nodes is higher than the bed elevation at both nodes, i.e., when $\min\left(z_{s,j}, z_{s,i}\right) > \max\left(z_{b,j}, z_{b,i}\right)$.

In a 2-D structured grid with a horizontal bed, the flux correction is equivalent to a centered discretization of a diffusion term with the form:

$$\sum_{j \in K_i} 0.5\sqrt{g h_{ij}}\,\Delta_{ij} L_{ij} \approx \frac{\partial}{\partial x}\left(\frac{c\Delta x}{2}\frac{\partial z_s}{\partial x}\right) + \frac{\partial}{\partial y}\left(\frac{c\Delta y}{2}\frac{\partial z_s}{\partial y}\right) \tag{9}$$

where $c = \sqrt{gh}$ is the celerity of gravity waves in shallow water flows. The flux correction has therefore the effect of damping high-frequency free surface oscillations.

The flux correction $0.5\sqrt{g h_{ij}}\,\Delta_{ij} L_{ij}$ introduced in equation (7) has a number of desirable properties. First, when the velocity tends to zero and the bed is horizontal it gives the same numerical flux as the scheme of Roe [*Cea et al.*, 2007], which means that the numerical dissipation under quasi-hydrostatic conditions is the same for both schemes. Second, the fact of computing the term Δ_{ij} applying the Minmod type limiter given by equation (8) guarantees that this term vanishes under hydrostatic conditions ($z_{s,j} = z_{s,i}$) as well as under uniform flow conditions ($h_j = h_i$), without the need of using an upwind discretization of the source terms, as it is the case in the scheme of Roe [*Bermúdez and Vázquez-Cendón*, 1994; *Cea et al.*, 2007]. On the other hand, the magnitude of the correction is significant in the presence of a hydraulic jump, where the difference in water surface elevation is large, contributing in this case to stabilize the solution. Third, it does not affect the mass conservation property of the scheme, since the flux correction is computed for each cell face and then added with the same absolute value but opposite sign to the two neighbor control volumes. Finally, equation (7) is very simple to compute and to implement, since it just requires a few additional simple operations compared to equation (5).

Since the discretization given by equations (3) and (4) is explicit in time, it is subject to a Courant-Friedrichs-Lewy (CFL) stability constraint over the computational time step [*Courant et al.*, 1967]. The CFL stability criterion establishes a relation between the maximum permissible computational time step, the grid size, the flow velocity and the water depth. Various slightly different definitions of the CFL condition have been proposed in 2D unstructured solvers for the shallow water equations, which mainly differ in the way in which the characteristic length of a grid cell is defined [*Guinot and Soares-Frazao*, 2006; *Marche et al.*, 2007; *Sanders et al.*, 2008; *Valiani et al.*, 2002; *Yoon*, 2004]. We have chosen here to define the computational time step as follows:

$$\Delta t = \min \Delta t_i \qquad i = 1, N \qquad\qquad \Delta t_i = \mathrm{CFL}\,\frac{\min_{j \in K_i} L_{ij}}{|\mathbf{U}|_i + \sqrt{g h_i}} \tag{10}$$

where $|\mathbf{U}|_i$ is the modulus of the water velocity at the cell C_i and N is the number of cells in the mesh. For numerical stability, the CFL must be lower than one. However, since the CLF stability criterion was derived for the linearized system of shallow water equations without source terms, values slightly smaller than one are often needed in practice due to the nonlinearity of the numerical schemes used to solve the shallow water equations and to the presence of source terms.

All the source terms in equations (3) and (4) are computed with a centered discretization scheme. The discretization of the rainfall intensity R_i and infiltration rate f_i will be treated in the next section. The free surface gradient $S_{x,i}$ is computed in each computational cell by means of the Gauss theorem as:

$$S_{x,i} = \sum_{j \in K_i} z_{s,ij} n_{x,ij} \qquad\qquad z_{s,ij} = \alpha_{ij} z_{s,i} + (1 - \alpha_{ij}) z_{s,j} \tag{11}$$

where $z_{s,ij}$ is an approximation of the free surface at the cell face, computed from linear interpolation between the adjacent control volumes C_i and C_j, and α_{ij} is the linear interpolation coefficient defined previously.

An explicit discretization of the bed friction term ($T_{x,i}$) in very shallow flows with depths of the order of a few mm or cm, over very rough terrains, might cause unrealistically large values of the shear stress, introducing a potential source for instability in the numerical algorithm. If this term is not carefully discretized it can further restrict the time step limitation given by equation (10), since the CFL condition is derived for the linearized shallow water equations with no source terms. For this reason, a semiimplicit bed friction discretization is commonly used in shallow water codes in order to improve the numerical stability when the water depth tends to zero [*Begnudelli et al.*, 2008; *Caleffi et al.*, 2003; *Cea and Vázquez-Cendón*, 2010, 2012; *de Almeida et al.*, 2012; *Guinot and Soares-Frazao*, 2006; *Sanders et al.*, 2008; *Valiani et al.*, 2002]. We have used the following semiimplicit discretization for $T_{x,i}$:

$$T_{x,i} = -g\left(\frac{n^2}{h^{7/3}}|\mathbf{q}|\right)_i^n q_{x,i}^{n+1} \tag{12}$$

Using equation (12) in equation (4), the unit discharge at time t^{n+1} on the computational cell C_i is computed as:

$$q_{x,i}^{n+1} = \frac{q_{x,i}^n - \sum_{j\in K_i} F_{x,ij}^n \frac{\Delta t}{A_i} - g h_i S_{x,i}^n \Delta t}{1 + g\left(\frac{n^2}{h^{7/3}}|\mathbf{q}|\right)_i^n \Delta t} \tag{13}$$

Equation (13) guarantees that the unit discharge tends smoothly to zero as the bed friction increases.

2.2. Wet-Dry Fronts

Wet-dry fronts are defined as the interface between dry and wet regions. A control volume face belongs to a wet-dry front if it joins a wet cell with a dry cell. For this purpose, dry cells are defined by means of a wet-dry tolerance parameter (ε_{wd}). If the water depth in a given cell is lower than the wet-dry tolerance parameter ($h_i < \varepsilon_{wd}$) the cell is considered to be dry. All the test cases presented in this paper were computed with a value of $\varepsilon_{wd} = 10^{-4}$m, since water depths smaller than this value are not physically relevant in realistic overland flow applications. Nevertheless, smaller values of ε_{wd} can be used with the DHD scheme without numerical stability problems, but they will not produce any improvement in the numerical solution while increasing the computation time.

The numerical treatment of wet-dry fronts in the DHD scheme only affects the computation of λ_{ij} (equation (5)) and $z_{s,ij}$ (equation (11)) at the control volume faces which belong to a wet-dry front. Assuming, without loss of generality, that the control volume C_i is wet and C_j is dry, the value of these variables at the cell face are computed as:

$$\lambda_{ij} = \begin{cases} U_{x,i} n_{x,ij} + U_{y,i} n_{y,ij} & \text{if } z_{b,j} < z_{s,i} \\ 0 & \text{if } z_{b,j} \geq z_{s,i} \end{cases} \tag{14}$$

$$z_{s,ij} = \begin{cases} \alpha_{ij} z_{s,i} + (1-\alpha_{ij}) z_{s,j} & \text{if } z_{b,j} < z_{s,i} \\ z_{s,i} & \text{if } z_{b,j} \geq z_{s,i} \end{cases} \tag{15}$$

The computation of λ_{ij} and $z_{s,ij}$ at wet-dry fronts implies that the water velocity and free surface gradient are equal to zero at the fronts in which the bed elevation of the dry node ($z_{b,j}$) is higher than the free surface elevation of the wet node ($z_{s,i}$). This assures that the fluxes of mass and inertia computed from equations (5) and (7) are also zero at the wet-dry fronts in which $z_{b,j} \geq z_{s,i}$. Otherwise, the velocity at the front is approximated as the velocity at the wet node and the free surface is computed from equation (11).

In addition, in dry cells all the source terms are set to zero except the rainfall rate in the mass conservation equation. No further special treatment of wet-dry fronts is required. The mass conservation property of the DHD scheme in the presence of wet-dry fronts is verified in Supporting Information S1.

2.3. Conservation of the Hydrostatic Solution

A desirable property of any numerical scheme used to solve the shallow water equations is its capacity to compute exactly the hydrostatic solution, i.e., to maintain water at rest with a constant free surface elevation. This property, which is usually called the C-property, was originally proposed in *Bermúdez and*

Vázquez-Cendón [1994] and it was afterward used in order to prove the so-called well-balance properties of shallow water solvers [*Cea et al*., 2007; *Kim et al*., 2008; *Liang and Marche*, 2009; *Liang*, 2010; *Marche et al*., 2007]. As proved in the following, the DHD scheme preserves the exact hydrostatic solution in problems involving irregular topography and wet-dry interfaces. This property of the scheme is also verified numerically in Supporting Information S1.

Under hydrostatic conditions, the water velocity is zero and the free surface elevation is constant at all the mesh nodes and edges. This implies that λ_{ij} and Δ_{ij} in equation (7) are also zero and therefore, the advective flux Q_{ij} is exactly zero at every cell edge. This provides an exact balance of the mass conservation equation (equation (3)) under hydrostatic conditions.

Regarding the momentum balance discretization (equation (4)), the zero velocity condition assures that the advective flux ($F_{x,ij}$) and the bed friction ($T_{x,i}$) discretizations are exactly zero at all the mesh edges and nodes, respectively. The free surface gradient discretization ($S_{x,i}$) also vanishes at every control volume, since under hydrostatic conditions the free surface elevation is constant ($z_{s,ij}=z_s=constant$) and the following geometric property applies to both the x and y components of any closed control volume:

$$S_{x,i}=\sum_{j\in K_i} z_{s,ij}n_{x,ij}=z_s\sum_{j\in K_i} n_{x,ij}=0 \tag{16}$$

The computation of $z_{s,ij}$ in wet-dry fronts using equation (15) guarantees that $S_{x,i}$ equals zero when the water is at rest, even in the presence of wet-dry interfaces and with irregular topographies. Since the discretizations of the advective flux, the bed friction and the bed surface gradient are zero, the momentum equation is exactly balanced under hydrostatic conditions.

2.4. Infiltration

In order to assure the positivity of the water depth in the presence of water layers of a few millimeters with high-infiltration rates, the mass conservation equation is solved in two steps. In the first step, an intermediate water depth is computed considering only the advective and rainfall terms in equation (4), as:

$$h_i^*=h_i^n-\sum_{j\in K_i} Q_{ij}^n\frac{\Delta t}{A_i}+R_i^n\Delta t \tag{17}$$

In the second step, the infiltration depth is subtracted from h_i^*. To assure that the water depth remains positive, the real infiltration rate is limited by the available content of water on each control volume as:

$$h_i^{n+1}=h_i^*-f_i\Delta t \qquad f_i=\min\left(f_i^{pot},h_i^*/\Delta t\right) \tag{18}$$

where f_i^{pot} is the potential infiltration rate, which might be computed explicitly from any standard infiltration formulation [*Chow et al*., 1988].

2.5. Boundary Conditions

The value of the water depth and unit discharges h_{ij}^U, $q_{x,ij}^U$, and $q_{y,ij}^U$ need to be defined at the control volume faces which belong to the mesh boundary in order to compute the mass and inertia fluxes in equations (3) and (4), as well as the free surface gradient with equation (11). For this purpose three types of boundaries are considered: inlet, outlet, and closed (wall) boundaries. In the following, we will assume that the cell C_i is a boundary cell and that the cell face L_{ij} is a boundary face.

At closed boundaries the normal component of the velocity and the free surface gradient are set to zero ($\lambda_{ij}=0$ and $z_{s,j}=z_{s,i}$), which implies that the mass and inertia fluxes are also zero ($F_{x,ij}=F_{y,ij}=Q_{ij}=0$).

At inlet boundaries, the two components of the unit discharge ($q_{x,ij}^U$ and $q_{y,ij}^U$) are always imposed by the user. In case of supercritical flow, the value of the normal velocity component (λ_{ij}) is also imposed by the user, while under subcritical flow conditions its value is extrapolated from the inner cell ($\lambda_{ij}=\lambda_i$). The value of the water depth is directly computed from the unit discharges and the normal velocity component as $h_{ij}^U=|\mathbf{q}|_{ij}^U/\lambda_{ij}$, where $|\mathbf{q}|$ is the modulus of the unit discharge at the boundary face imposed by the user ($|\mathbf{q}|_{ij}=\sqrt{q_{x,ij}^2+q_{y,ij}^2}$).

At outlet boundaries the unit discharges ($q_{x,ij}^U$ and $q_{y,ij}^U$) are extrapolated from the inner cell ($q_{x,ij}^U=q_{x,i}$ and $q_{y,ij}^U=q_{y,i}$), while the water depth (h_{ij}^U) is imposed by the user in case of subcritical flow and extrapolated from the inner cell ($h_{ij}^U=h_i$) in case of supercritical flow.

In most of the test cases presented in this paper there are no inlet boundaries, since the overland flow is generated directly by the rainfall input. Regarding the outlet boundary, a critical flow condition was used in all the test cases. This is equivalent to an outlet boundary condition in which the water depth at the boundary is computed as $h_{ij}^U = \left(|\mathbf{q}|_i^2/g\right)^{1/3}$, where $|\mathbf{q}|_i$ is the modulus of the unit discharge at the inner node.

2.6. Other Discretizations Used in This Work

In the results section, the DHD scheme will be compared to three other numerical approximations for overland flow computations, which in increasing order of complexity are: the diffusive wave (DW) model, the simple inertia (SI) formulation, and the Roe scheme applied to the shallow water equations [*Toro*, 2001]. Compared to the full shallow water model, the SI formulation neglects the advective inertia in the momentum conservation equations [*Bates et al*., 2010; *Ponce*, 1990], while the DW formulation neglects both the local and advective inertial terms. The DHD scheme solves the full shallow water model and therefore, in terms of process representation is similar to the scheme of Roe. However, as argued in previous sections the numerical discretization is simpler and therefore, in terms of numerical complexity it can be placed between the SI and Roe schemes. Previous publications [*de Almeida and Bates*, 2013] have shown that the SI equations are appropriate for flood inundation modeling and gradually varied subcritical flow, and work best when the Froude number is less than 0.5. As the Froude number increases toward 1 the SI solution deteriorates as explored in *de Almeida and Bates* [2013]. This is also the case of the DW model [*Hunter et al*., 2007], and for this reason both models have not been used for comparison in the test cases involving generalized supercritical flow conditions. *Hunter et al*. [2007] proposed the ratio of bed shear to advection forces as an indicator of the applicability of the DW approximation. From dimensional analysis of the shallow water equations, this ratio (R_f) can be defined as:

$$R_f = \frac{L_0 g n^2}{h_0^{4/3}} \tag{19}$$

where h_0 and L_0 are, respectively, representative values of the water depth and horizontal length scales. Values of R_f much larger than one imply that the bed friction force is more relevant than the advective acceleration and thus, the DW model is an appropriate approximation.

The mass conservation equation solved by the four schemes to compute the evolution of the water depth is the same one given in equations (1), which is discretized as indicated in equation (3). As mentioned before, cell outflows (Q_{ij}) are always equal to the inflows of the neighbor cells, which guarantees the global conservation of the mass of water in the four schemes. The main difference between the schemes is the approximation made in the momentum conservation equations in order to compute the water velocity, and the way in which the fluxes Q_{ij} and F_{ij} are discretized. The differences between the schemes are detailed in the following.

The scheme of Roe is a Godunov type scheme for hyperbolic systems of conservation laws which solves the full dynamic wave model, but contrary to the DHD scheme it solves the mass and momentum conservation equations as written in (1). Godunov's schemes are probably the most extended numerical methods for solving the shallow water equations [*Toro*, 2009]. They have proved to be very robust and accurate in problems involving unsteady hydraulic jumps, but they lead to complex upwind discretizations of the mass and momentum fluxes and of the source terms in order to achieve well-balanced schemes that preserve the stationary states of water at rest and uniform flow. The literature regarding the application of Godunov's methods to flood inundation modeling is very extensive. The reader is referred to the references mentioned in section 2.1 for a detailed description of recent developments and applications.

The idea behind the SI formulation is to avoid the numerical problems related to the DW approximation, which come from the fact of neglecting all the inertial terms in the momentum conservation equations, and at the same time to reduce the complexity of the numerical schemes used to discretize the advection terms in the momentum conservation equations. The SI formulation retains only the local acceleration (time derivative) of the inertial terms and neglects the advective acceleration (spatial derivative). The result is a momentum conservation equation which might be seen either as a simplification of the full shallow water equations or as an extension of the DW approximation. The simplified x momentum equation solved in the SI formulation is given by:

$$\frac{\partial q_x}{\partial t} = -gh\frac{\partial z_s}{\partial x} - gh\frac{n^2|\mathbf{q}|}{h^{10/3}}q_x \tag{20}$$

with an analogous equation for the *y* momentum.

The DW formulation goes one step further in process simplification, and computes the water velocity from the following uniform flow equations:

$$\frac{\partial z_s}{\partial x} = -\frac{n^2|\mathbf{q}|U_x}{h^{10/3}} \qquad \frac{\partial z_s}{\partial y} = -\frac{n^2|\mathbf{q}|U_y}{h^{10/3}} \tag{21}$$

Equation (21) assumes that the gravity force over the mass of water and the bed friction are in perfect balance at every time step during the simulation, neglecting therefore all inertial effects.

Several implementations of the SI and DW formulations have been proposed in the literature. For instance, *Bates et al*. [2010] and *de Almeida et al*. [2012] proposed recently several finite difference discretizations for the SI model in staggered structured grids. The DW has also been used in many hydrological studies, given rise to different implementations [*Cea et al*., 2010a; *Hunter et al*., 2007; *Leandro et al*., 2014]. In this work, all the formulations have been implemented in the same finite volume code in order to use the same unstructured grids when comparing the models. This comparison strategy is focused only in the different way in which the discrete flow equations are approximated, and it is optimal in order to minimize any differences in the implementation structure of the models. However, it has some implications regarding computation time. In general a simple scheme can be coded (or parallelized) in a more efficient way than a complex scheme. Also, the computational cost of structured and unstructured implementations is different. In this sense, an optimized *stand alone* implementation of each scheme would probably be coded in a more efficient way regarding memory and CPU time requirements. It is not the purpose of the present paper to analyze and compare the efficiency of different code implementation and parallelization strategies for the DHD, Roe, SI, and DW schemes.

Turning to the specific discretization used in this work, the SI formulation is very easily implemented as a variation of the DHD scheme, by just not computing the term $F^n_{x,ij}$ in equation (4). The number of operations per time step is slightly lower than those required by the DHD scheme, since the term $F^n_{x,ij}$ is not computed. Regarding the implementation of the DW model, the numerical scheme used is detailed in *Cea et al*. [2010a]. This discretization scheme is very similar to the one used in *Leandro et al*. [2014].

Another feature of each formulation which should be mentioned is the numerical stability requirements. All the discretizations used in this work are explicit in time, which implies that the computational time step is constrained by a stability condition. The maximum permissible time step for numerical stability in the full shallow water model is given by the CFL condition (equation (10)). This condition applies to the DHD and Roe schemes, since both of them solve the dynamic wave equations. Since the SI formulation neglects the advective acceleration, the stability condition is similar to that of the dynamic wave model, but dropping the velocity from the denominator [*Bates et al*., 2010; *de Almeida et al*., 2012]:

$$\Delta t_i = \mathrm{CFL}\frac{\min_{j\in K_i} L_{ij}}{\sqrt{gh_i}} \tag{22}$$

For the same CFL value, this condition allows larger time steps than equation (10), which contributes to diminish the computation time of the SI formulation compared to the DHD scheme.

The stability condition of explicit discretizations of the DW model is given by *Bates et al*. [2010], *Cea et al*. [2010a], *Hunter et al*. [2008], and *Schubert et al*. [2008]:

$$\Delta t_i \leq \Delta x_i^2 \frac{n_i}{h_i^{5/3}} \sqrt{\left(\frac{\Delta z_s}{\Delta x}\right)_i} \tag{23}$$

Comparing the stability conditions for the DW, SI, and dynamic wave models, which are given, respectively, by equations (10), (22), and (23), it is clear that the DW model will run faster in coarse meshes, while the dynamic wave and SI models will achieve a better efficiency at fine mesh resolutions. This is because the maximum stable time step in the DW model decreases quadratically with the mesh size while it decreases linearly in the case of inertial models. Moreover, the DW model is conditionally unstable as the free surface

slope or the bed roughness coefficient tends to zero, unless a limiter is used in the evaluation of the discharge between neighbor cells [*Hunter et al*., 2005]. This kind of discharge limiter improves the numerical stability and allows for larger time steps in the numerical solution, but at the same time it reduces the model accuracy. In the present simulations, the discharge limiter in the DW model was implemented as in *Cea et al*. [2010a].

3. Test Cases and Results

This section evaluates the DHD scheme in five cases involving overland flow over topographies of different complexity and spatial resolution. In addition to the five validation cases presented here, Supporting Information S1 contains some simple verification tests which prove the numerical stability and mass conservation property of the DHD scheme. The flow conditions in the test cases T1 and T2 are typical from urban environments, with high Froude numbers, fine mesh resolutions, a smooth bed surface, and relatively small bed slopes. The DHD and Roe discretizations are therefore more appropriate for these cases than the DW and SI formulations. The latter formulations have been used to compute the test case T1, but not T2, since it involves strong hydraulic jumps which cannot be reproduced by simplified inertia or purely diffusive formulations. The test cases T3 and T4 involve rainfall-runoff transformation in small rural basins. Compared to test cases T1 and T2, these tests are characterized by coarser mesh sizes, much rougher terrains, larger bed slopes, and in general Froude numbers smaller than one. The last test case is a dam break simulation with generalized supercritical flow conditions which are only affordable for a dynamic wave model. Thus, only the DHD and Roe schemes are compared in this last test.

In order to minimize the differences in the numerical implementation of the schemes, the four of them have been implemented in the shallow water model Iber [*Bladé et al*., 2014] and therefore, they share the same code structure. In all cases, the same finite volume mesh was used with the four schemes. Since all the implementations used in this work are explicit in time, the time step was limited by the stability condition given by equation (10) in the Roe and DHD schemes, equation (22) in the SI scheme and equation (23) in the DW scheme. The CFL was systematically set to a value of 0.9 in all the simulations, which in most cases produced stable results. In very few cases, the use of a CFL = 0.9 caused instabilities with a specific scheme, and the CFL value was lowered to 0.7. This was the case of the DHD and SI schemes in the test case T1 and of the Roe scheme in the test case T4. Using a CFL value equal to or larger than 1 caused systematically numerical instabilities in the solution with all the schemes.

In the following, we will first focus the analysis on the results obtained with the different numerical discretizations, and at the end of this section we will compare the CPU time requirements of each implementation.

3.1. Test Case T1: Rainfall-Runoff Over a Laboratory Simplified Urban Configuration

In this test case, a series of laboratory tests involving rainfall-runoff transformation in a simplified urban configuration are simulated with the four numerical schemes. The experimental setup was presented in *Cea et al*. [2010a]. Here we will use the experimental data registered in the so-called configuration A20, which consists of 20 blocks of 20 cm $\times$ 30 cm and 20 cm height randomly distributed over a 5 m^2 impervious basin (Figure 2). The bed of the basin in these experiments was made of steel and had some small microrugosities due to the deterioration of the surface and the accumulation of dust. Three hyetographs with intensities of 84, 180, and 300 mm/h will be used to evaluate the performance of the numerical schemes, and will be referred to as T1-R84, T1-R180 and T1-R300. In all of them, the rainfall intensity is constant during the first 20 s of the experiment and then it suddenly stops. At the beginning of the experiment all the domain is dry. The numerical mesh used in the computations is unstructured with approximately 3600 elements, the average mesh size being 4 cm (Figure 2). At the outlet boundary a critical flow condition is imposed, which represents correctly the experimental conditions.

Figure 3 shows the spatial distribution of the maximum Froude number computed during the whole simulation for the rain intensities of 84 and 300 mm/h. In most of the basin the maximum Froude number reaches values near to or larger than 1, with maximum values slightly larger than 2 in very few locations. This suggests that a priori the SI and DW formulations might not be appropriate for this test case, since both of them neglect the advective acceleration terms in the momentum equations. In addition, the surface runoff is intercepted by an obstacle located near the basin outlet, generating a small pond in which the water surface elevation is almost constant. This is a handicap for the DW formulation since its computational time

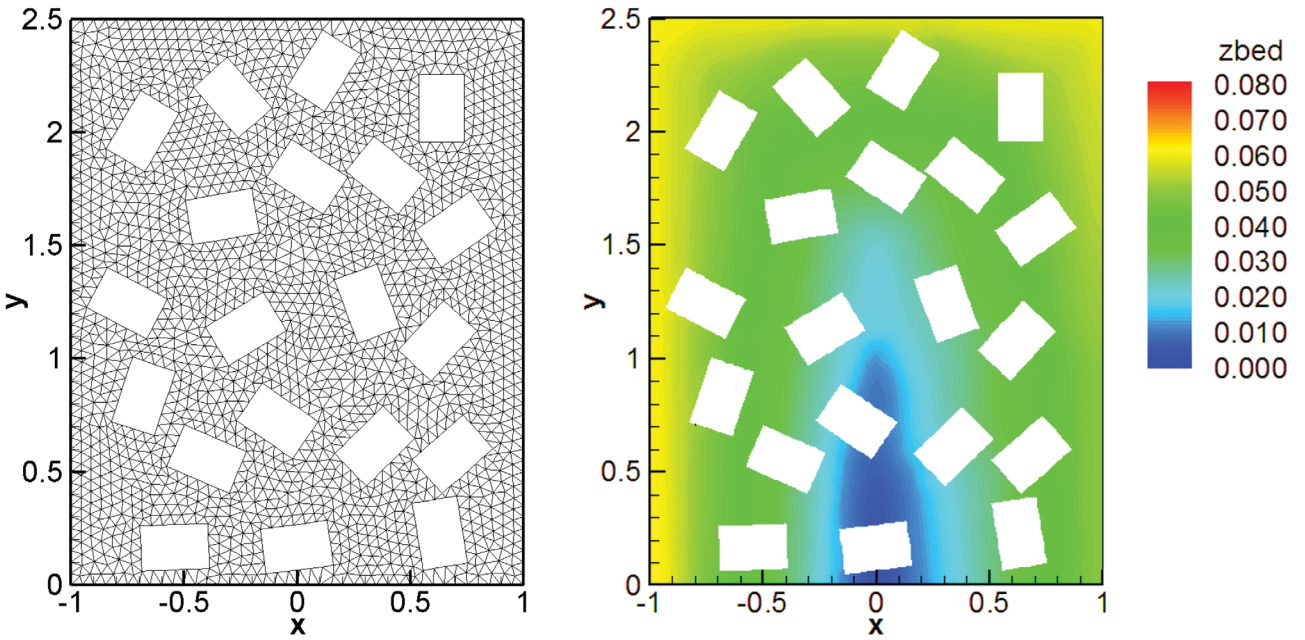

Figure 2. Test case T1. (left) Numerical mesh and (right) topography.

step is subject to the stability constraint given by equation (23), which is proportional to the water surface slope.

The Manning coefficient was calibrated independently for each numerical scheme, in all cases for the intensity of 84 mm/h. The manually calibrated coefficients were $n = 0.016$ for the DHD and Roe schemes, and $n = 0.027$ for the SI and DW models. With these bed friction coefficients the agreement with the experimental data obtained with the four schemes is good for the three rainfall intensities (Figure 4). The DHD and Roe schemes produce very similar outlet hydrographs using the same Manning coefficient. Considering that the bed surface of the basin is smooth, a Manning coefficient of 0.016 (as obtained from the calibration of the DHD and Roe schemes) is more realistic in this case than a value of 0.027. The fact of needing a higher Manning with the SI and DW formulation is due to the fact of neglecting the advective terms in the momentum equations. The strong curvature of the flow paths forced by the spatial disposition of the obstacles in the basin as well as the high maximum Froude numbers achieved during the computation (Figure 3) increases the relevance of the advective terms in this case and invalidates the application of the SI and DW schemes [*de Almeida and Bates*, 2013]. In the calibration of the latter models, the effect of the advective forces is absorbed by the bed friction, and this is probably the reason why the calibrated Manning coefficient is higher in these formulations. To a certain degree, the calibration of the Manning coefficient is partially accounting for the inaccuracies of the mathematical model. Quite surprisingly, in spite of these limitations the hydrographs predicted by the DW and SI models with $n = 0.027$ are in good agreement with the experimental data (Figure 4).

3.2. Test Case T2: Overland Flow in a Four-Branch Junction

In the second test case, the flow field in a 90° four-branch open-channel junction under steady supercritical flow conditions is computed. The geometry and dimensions of the junction are shown in Figure 5. The slope of the channels aligned with the x and y axis are, respectively, 0.01 and 0.02 m/m, while the junction itself is a horizontal square 1.5 m wide. The bed surface is made of concrete. The inlet discharges for both channels are respectively $Q_{in,x} = 0.0429 \mathrm{m}^3/\mathrm{s}$ and $Q_{in,y} = 0.100 \mathrm{m}^3/\mathrm{s}$. The configuration and flow conditions of this test case are typical from surface drainage in urban environments. A thorough description of the setup and experimental methodology can be found in *Nanía et al*. [2011].

Under the experimental flow conditions, the flow is subcritical in the inlet aligned with the x axis and supercritical in the inlet aligned with the y axis, and an oblique hydraulic jump is formed in the junction.

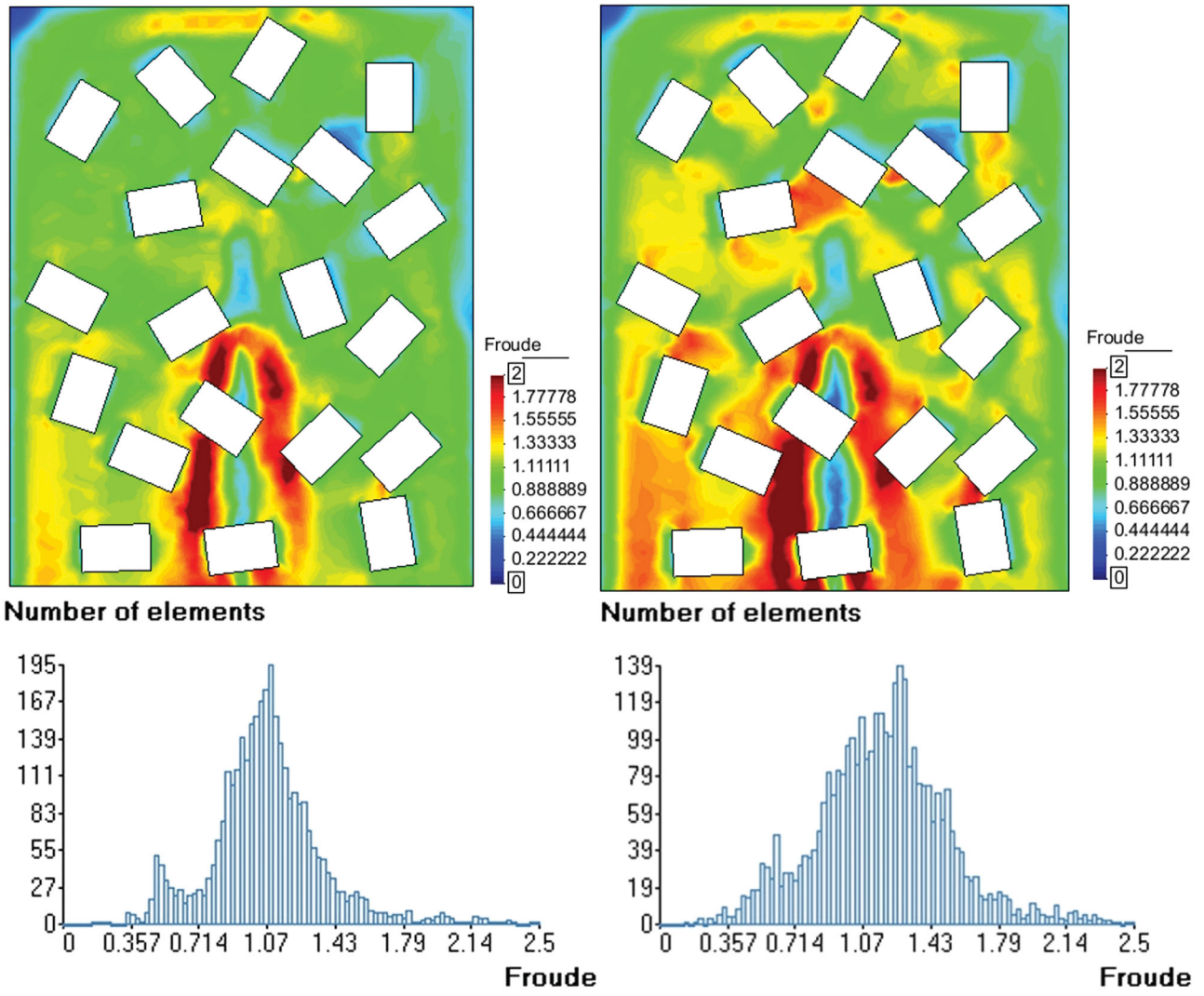

Figure 3. Test case T1. Spatial and frequency distribution of the maximum Froude number at each computational cell during the whole simulation. The results shown correspond to the test cases (left) T1-R84 and (right) T1-R300 computed with the numerical scheme of Roe.

Downstream the junction the flow returns to supercritical conditions in both channels. Due to the presence of the oblique hydraulic jump and Froude numbers which vary from 0.2 to 4 inside the domain, the SI and DW models are not appropriate for this case and therefore, they have not been considered in the schemes comparison, which is only presented for the DHD and Roe schemes.

The finite volume grid used in the numerical computations has 6480 rectangular elements. A Manning coefficient of $n = 0.016$, which is a typical value for concrete surfaces, was used in all the computations without any calibration. The total discharge was imposed at both inlet boundaries. In addition, a critical depth condition was imposed at the inlet aligned with the y axis, in which the flow is supercritical. Since the flow is supercritical downstream the junction, the water depth and velocity do not need to be imposed at the outlet boundaries.

As it should be expected, the scheme of Roe gives a sharper definition of the hydraulic jump than the DHD scheme, which in general predicts a smoother variation of the free surface elevation and velocity, as shown in the longitudinal profiles represented in Figure 6. Despite these differences in the results obtained with both schemes, the DHD predicts correctly the position and strength of the hydraulic jump, and the global agreement with the experimental data is very satisfactory for both schemes, as shown in Figure 5.

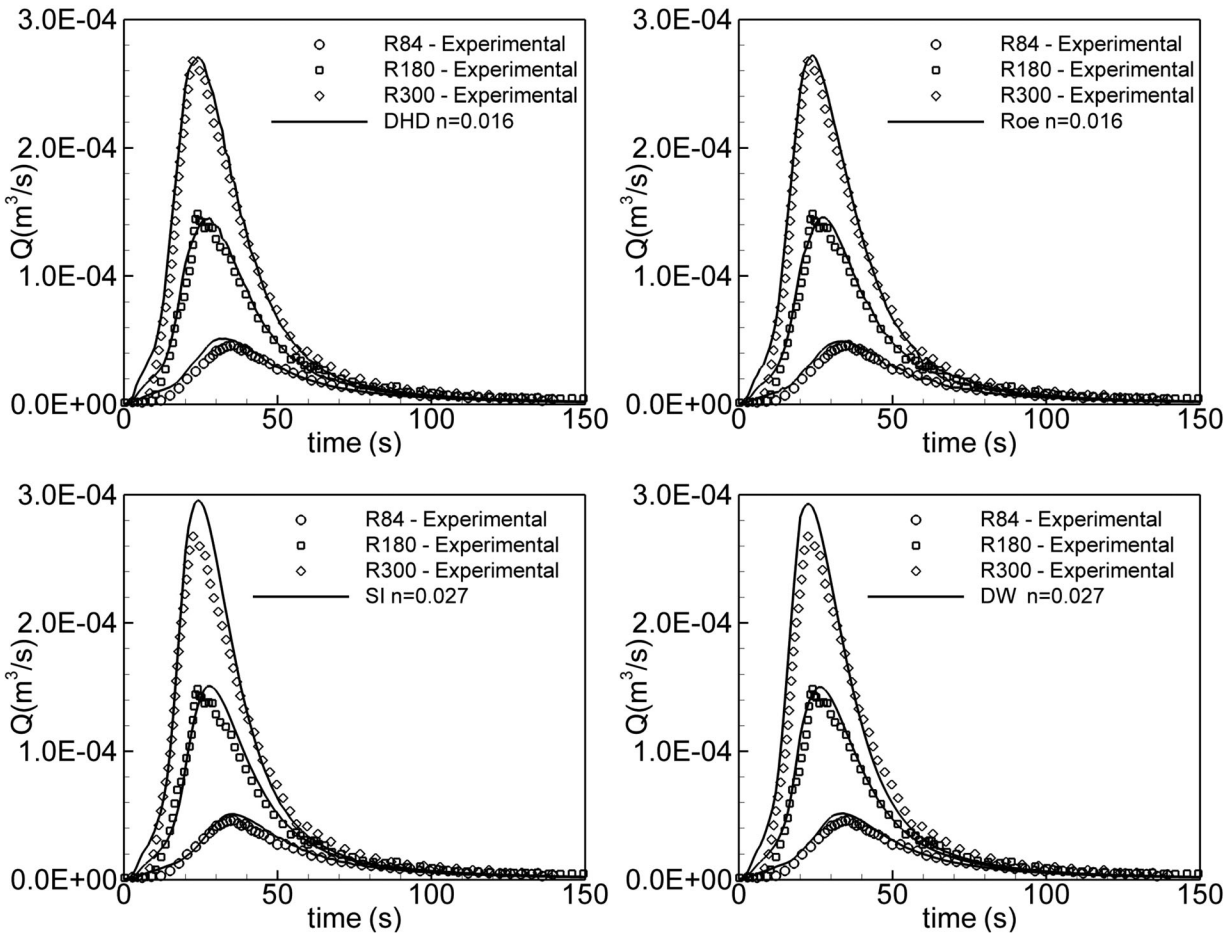

Figure 4. Test case T1. Experimental and numerical outlet hydrographs.

3.3. Test Case T3: The Solivella Catchment

In this test case, we compute the hydrograph generated by a 4 h storm event with a 100 year return period in the Solivella catchment, which is a 4 km^2 rural basin located in the North-East of Spain. The flow conditions of this test case are rather different from the previous ones and favor the application of the DW and SI formulations, since it involves much higher bed roughness values and larger bed slopes, boosting the relevance of these terms in the momentum balance. The mesh size used in the simulations is also much larger than in the previous test cases, which is an additional advantage for the DW formulation since the stable time step for this model increases with the square of the mesh size as defined in equation (23).

The bed elevation in the watershed varies from 500 m at the catchment outlet to 760 m in the upper areas (Figure 7), with maximum bed slopes of 0.7 m/m. The presence of different types of vegetation and microtopography features which are not resolved by the DTM increase the value of the effective roughness coefficient, which has to account for all these unresolved features. Manning numbers much larger than those commonly used in river hydraulics applications, and which depend on the vegetative cover, the microtopography, the rainfall intensity and the water depth have been previously reported in computations involving rainfall-runoff transformation over rough terrains [*Engman*, 1986; *Fraga et al*., 2013; *Muñoz-Carpena et al*., 1999; *Wilson et al*., 2002]. Since no calibration data are available for this test case, the same Manning coefficient was used with all the schemes, which was fixed to a value of 0.15, constant in the whole catchment. The design hyetograph was evaluated using the alternating block method with a block length of 15 min, the maximum precipitation intensity being 140 mm/h. Infiltration was assumed to be negligible, which corresponds to initial conditions of fully saturated soil with a very low permeability.

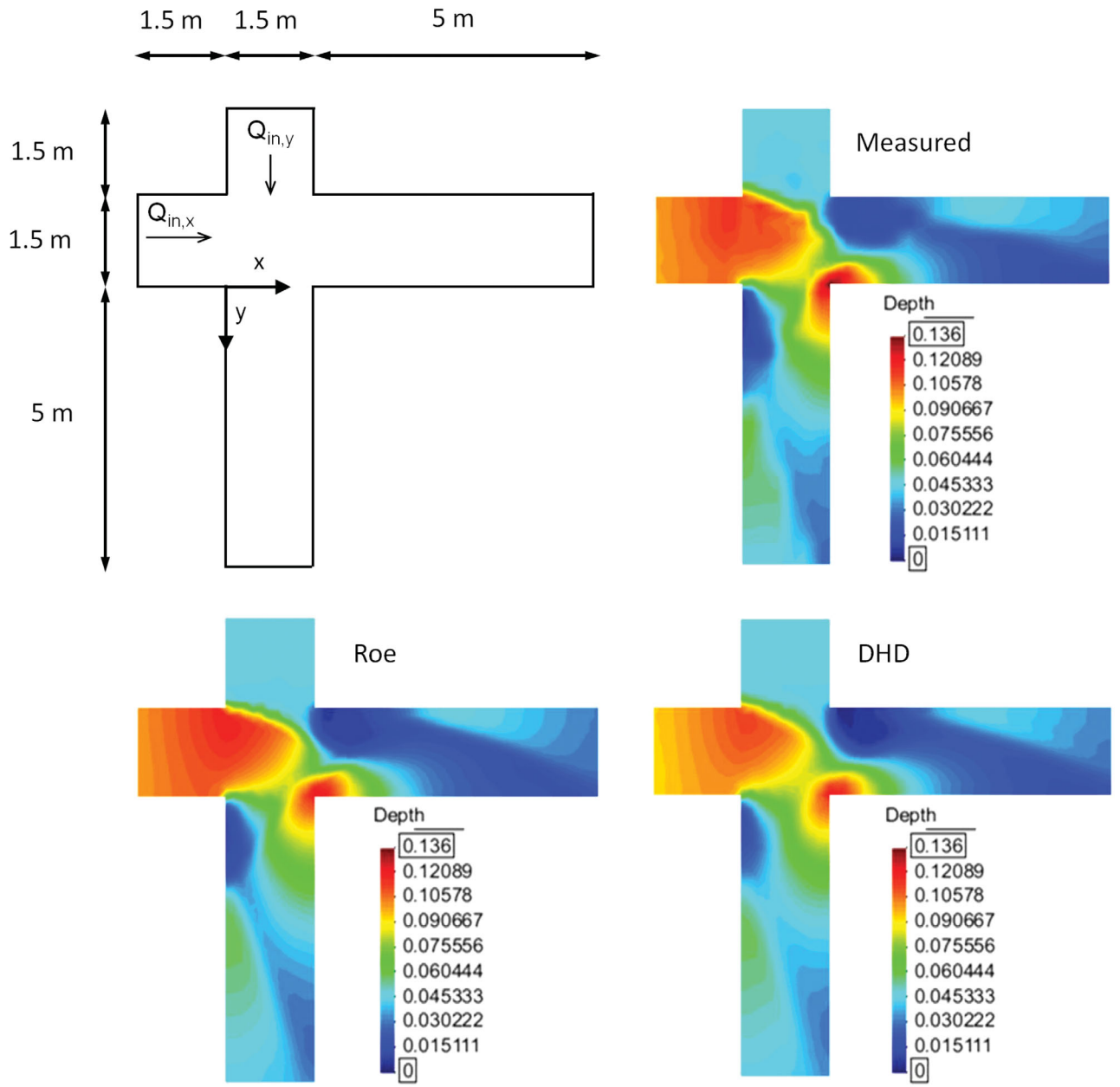

Figure 5. Test case T2. (top, left) Geometry of the four-branch junction, (top, right) measured water depth field, (bottom, left) water depth field computed with the scheme of Roe, and (bottom, right) water depth field computed with the DHD scheme.

The catchment was discretized with an unstructured Right-Triangulated Irregular Network (RTIN) mesh [*Evans et al.*, 2001] with 17,926 elements, the average element area being 240 m^2. A critical flow condition was imposed at the basin outlet.

The shape of the outlet hydrographs computed with all the schemes is very similar (Figure 7), which is coherent with the fact that the configuration of this test case implies that the bed friction and slope terms are the most relevant in the momentum equations, while the advective acceleration has a much lower relevance in the solution. Taking the characteristic length scale as the average mesh size ($L_0 = 20$ m) and the representative water depth as the average water depth in the watershed ($h_0 = 0.1$ m), the ratio of the bed shear to advection obtained from equation (19) is of the order of $R_f \approx 100$, which highlights the importance of bed friction in this test case.

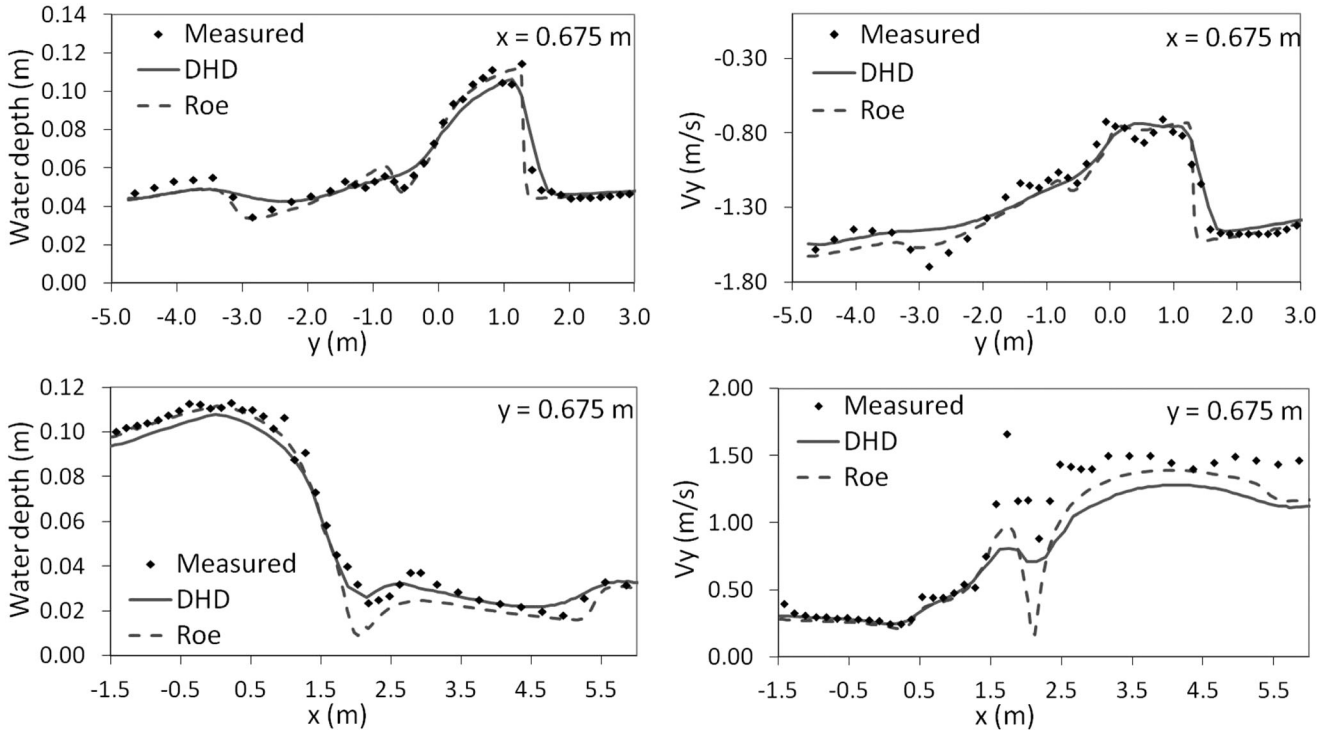

Figure 6. Test case T2. Experimental and numerical profiles of water depth and velocity. (top, left) Water depth at $x = 0.675$ m, (top-right) V_y at $x = 0.675$, (bottom, left) water depth at $y = 0.675$ m, and (bottom, right) V_x at $y = 0.675$.

Using the same Manning coefficient, the hydrographs predicted by the DHD and SI schemes overlap (Figure 7), the peak discharge (90 m^3/s) being slightly larger than the one obtained with the scheme of Roe (84 m^3/s). Nonetheless, the differences obtained with the DHD and Roe schemes are minor. Moreover, the computed basin lag time is the same for both schemes. The DW approximation predicts a slightly larger peak discharge (94 m^3/s), but the differences with the other schemes in the global shape of the hydrograph are negligible for this kind of application.

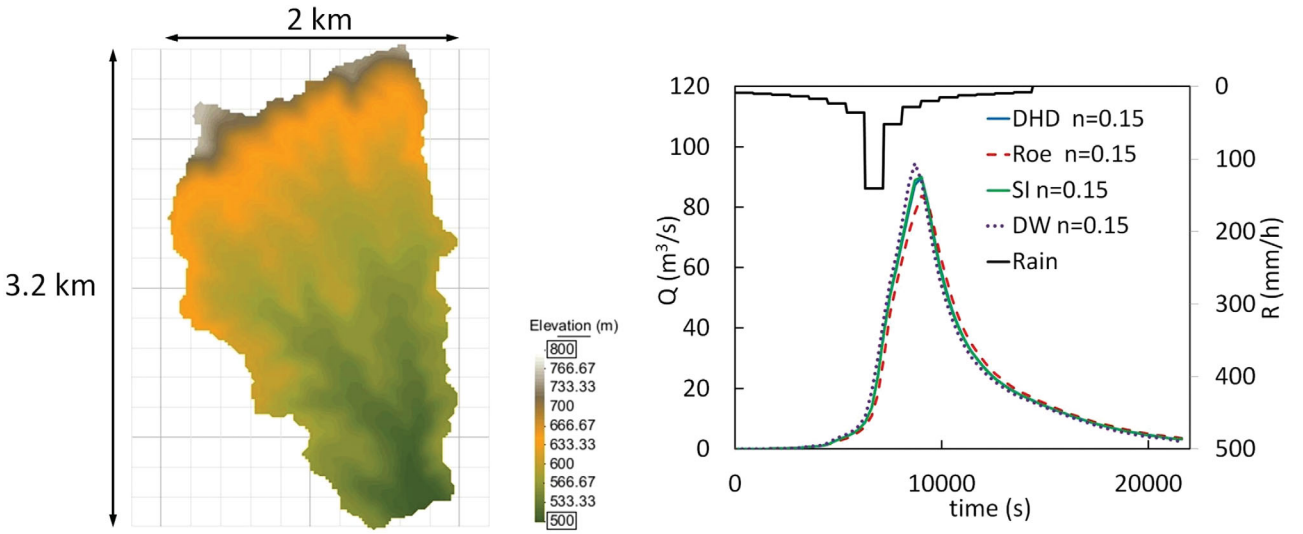

Figure 7. Test case T3. (left) Topography of the Solivella catchment and (right) numerical hydrographs computed at the basin outlet for a 4 h design storm with a 100 year return period. DHD and SI results overlap.

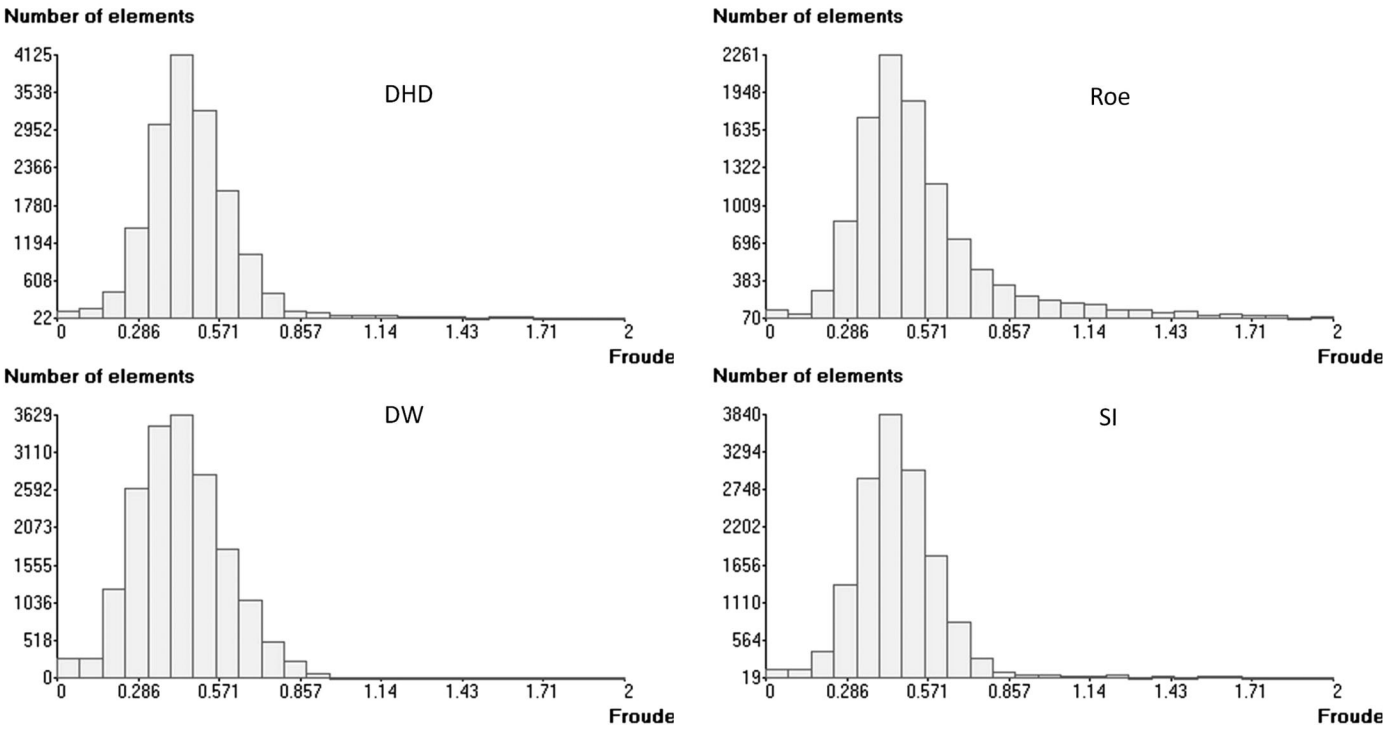

Figure 8. Test case T3. Frequency distribution of the maximum Froude number at each computational cell during the whole simulation. (top, left) DHD, (top, right) Roe, (bottom, left) DW, and (bottom, right) SI.

Figure 8 shows, for each scheme, the frequency distribution of the maximum Froude number computed at each mesh cell during the whole simulation. The distributions obtained with the four schemes are very similar, with an average value of the order of 0.4 and very few cells in which the Froude number exceeds the value of 1. The DW model tends to give slightly lower Froude numbers and the Roe scheme somewhat larger values. These values are coherent with the fact that the SI and DW models perform well in this test case.

3.4. Test Case T4: The Maior River Catchment

This test case consists on the computation of the hydrograph generated during a storm event in a rural catchment of approximately 5 km^2, located in the North-West of Spain. The topography of the catchment is very steep, the average and maximum bed slopes in the whole basin being 0.34 m/m and 0.90 m/m, respectively. The bedrock, composed mainly of fractured granite, is very near the soil surface, which is mainly covered by bushland and scrubs.

The unstructured numerical mesh used in the computations has 24,676 triangular elements, with an average element size of 20 m. The mesh is coarser in the hillslopes (30 m) and finer in the main water streams (10 m), as shown in Figure 9. The only boundary condition imposed in the model is a critical flow condition at the basin outlet. Rainfall data with a time resolution of 5 min were obtained from a rain gauge located near the basin outlet. Given the relatively small size of the catchment, a spatially uniform rainfall intensity was assumed in the computations. At the beginning of the rainfall event, the soil was completely saturated due to the continuous precipitations in the previous days. For that reason, a very simple model for rainfall losses was used for calibration, the only infiltration parameter being the constant infiltration rate. The second parameter used for calibration is the Manning coefficient.

Groundwater base flow was not considered in the numerical model, since it is not the aim of the work presented in this paper. However, in this test case its contribution to the outlet hydrograph is not negligible and therefore, it has been roughly determined from the measured discharge. Before the rainfall event starts the discharge in the main stream was 0.2 m^3/s, while the end of the recession limb tends to a quasi steady

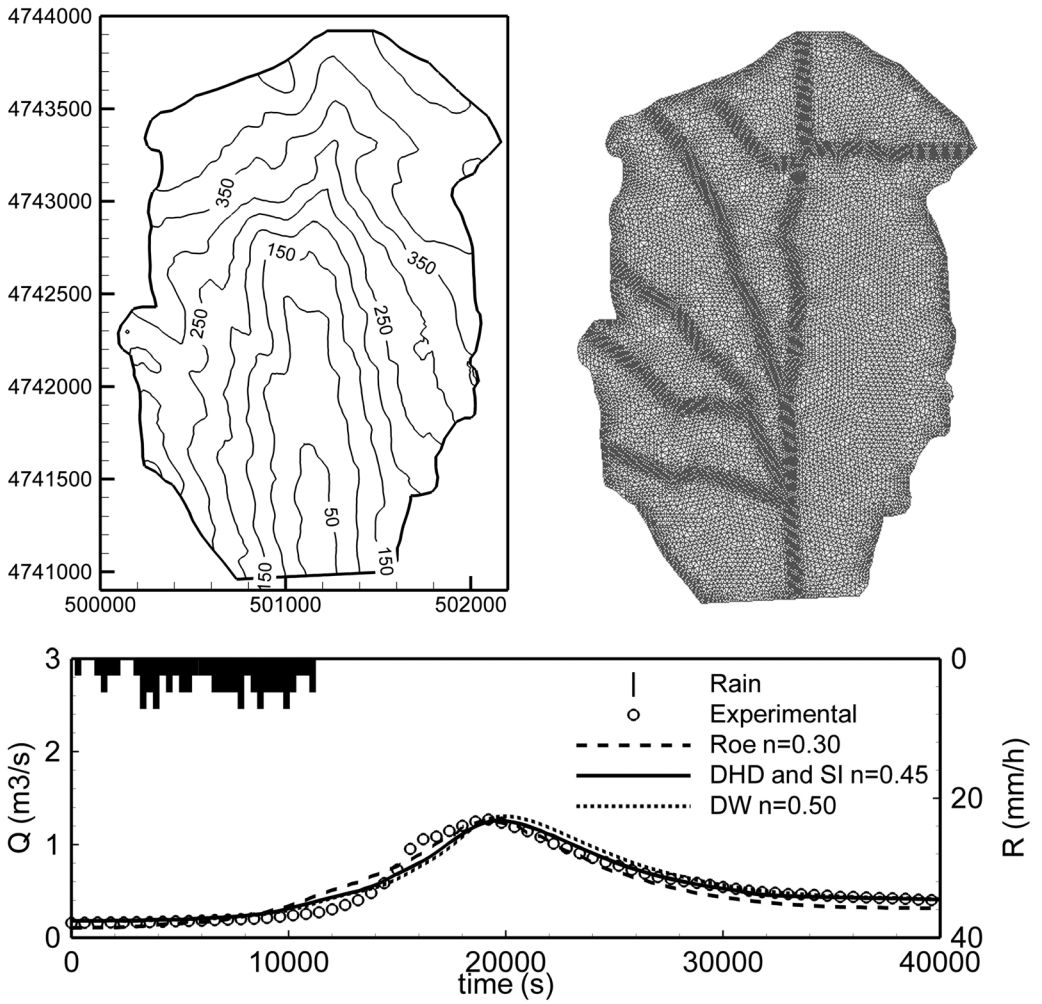

Figure 9. Test case T4. (top, left) Catchment topography, (top, right) finite volume mesh, and (bottom) outlet hydrographs computed with the four schemes. DHD and SI results overlap.

value of 0.4 m^3/s (Figure 9). In order to account in the numerical model for the base flow contribution in a simple way, and considering that the aim of this test case is just to evaluate the performance of the discretization schemes for the surface runoff and not to analyze the hydrologic behavior of the catchment, we have imposed a linear variation of the river discharge from 0.2 to 0.4 m^3/s during the event. This discharge, which is added to the rainfall-runoff contribution, is imposed directly in the numerical model as a point source in the main water stream.

The maximum Froude number at each cell during the whole computation never reaches values larger than 1 at any spatial location (Figure 10), and it exceeds the value of 0.4 in just 10% of the basin surface, which is a first requirement for the validity of the DW and SI formulations.

After manual calibration of the constant infiltration rate and Manning coefficient, the four numerical discretizations produce a correct prediction of the measured hydrograph (Figure 9). The DHD and SI formulations produce virtually the same results using the same Manning ($n = 0.45$ $sm^{-1/3}$) and infiltration rate ($f = 1.9$ mm/h) parameters. This is because the ratio of bed friction to advection is in this case of the order of $R_f \approx 50$ in the main river streams, where it attains its lower values due to the larger water depth and smaller mesh size. In the hillslopes, its value is even larger because the numerical mesh is coarser and the water depth smaller. The bed friction and topography are therefore the most relevant terms in the momentum balance, and both schemes use the same discretization for those terms. The scheme of Roe produces slightly different results, but with the same degree of accuracy. While the same infiltration rate was used with the scheme of Roe ($f = 1.9$ mm/h), the Manning coefficient had to be calibrated to a lower value

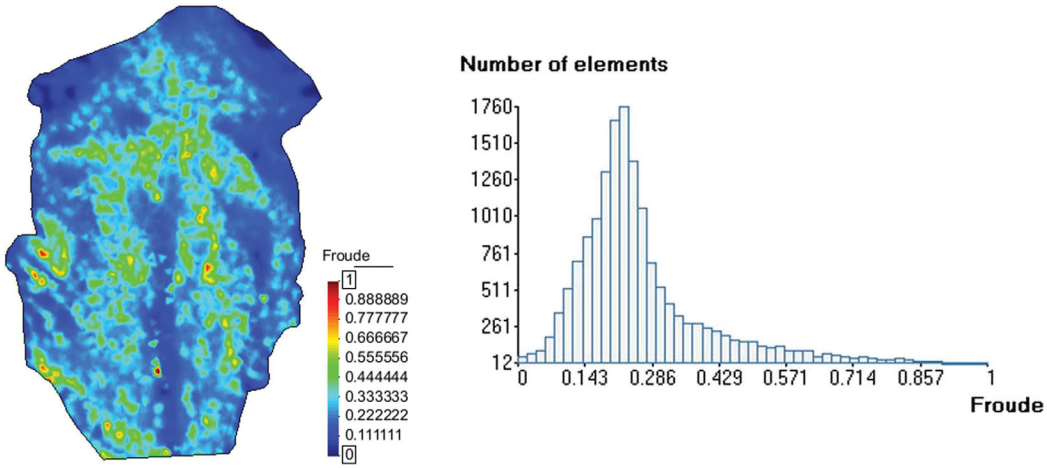

Figure 10. Test case T4. Spatial and frequency distribution of the maximum Froude number at each computational cell during the whole simulation. The results shown correspond to the DHD scheme.

($n = 0.30$ sm$^{-1/3}$) in order to correctly reproduce the outlet hydrograph. As for the DW model, it also shows a good agreement with the field measurements but using a higher Manning coefficient ($n = 0.50$).

These results highlight the impact of the numerical discretization on the calibrated Manning coefficient. Since in this case, the advection forces are of minor importance, the only difference between the Roe, DHD, SI, and DW schemes is the way in which the bed slope, hydrostatic pressure gradient, and bed friction terms are discretized. It could be argued that the discretization used in the DHD and SI schemes is more appropriate for this application since the hydrostatic pressure gradient and bed slope are merged in a single term (equation (2)) which is then discretized with a centered scheme (equation (11)). This minimizes the discretization errors introduced in the momentum balance when using different approximations for each term, as it is the case of the scheme of Roe, which uses different discretizations for the hydrostatic pressure (included in the momentum flux in equation (1)) and the bed slope. In fact, this is the reason why upwind discretizations of the bed slope are necessary in order to maintain the hydrostatic solution when using the scheme of Roe [*Bermúdez and Vázquez-Cendón*, 1994]. In addition, the Manning coefficients calibrated with the DW, SI, and DHD models are coherent with each other.

3.5. Test Case T5: Dam Break With an Obstacle

The last test case is intended to analyze the behavior of the scheme under the presence of a strong unsteady hydraulic jump. For this purpose, the experimental setup presented in *Soares-Frazão and Zech* [2007] has been used to model a 2-D dam break wave which hits an oblique rectangular obstacle placed downstream the dam, inducing the generation of an hydraulic jump just upstream the obstacle and a wake zone downstream. A schematic representation of the problem geometry is shown in Figure 11, while a thorough description of the experimental setup and results can be found in *Soares-Frazão and Zech* [2007]. The initial water depths are 0.40 and 0.02 m up and downstream the dam, respectively. The dam break is modeled by an instantaneous gate opening, and the experiment lasts 30 s. The Froude number reaches maximum values well above one over the whole domain and therefore, only the DHD and Roe schemes have been used to model this test case.

The finite volume mesh used in the computations has around 11,000 elements (most of them quadrilaterals), with an average mesh size of 10 cm in the region between the dam and the obstacle. The Manning coefficient was fixed to 0.01 sm$^{-1/3}$, which is the value recommended in *Soares-Frazão and Zech* [2007], without any further calibration. At the outlet of the experimental channel, a critical depth condition was imposed, although this boundary condition has no influence in the results since it is located 25 m downstream the obstacle [*Soares-Frazão and Zech*, 2007].

Overall, the Roe and DHD schemes give very similar velocity results (Figure 11), although the definition of the hydraulic jump is sharper with the scheme of Roe. Also, the DHD produces a very small spurious edge along the x axis in the velocity field. These differences are normal, since the DHD is simpler than the scheme

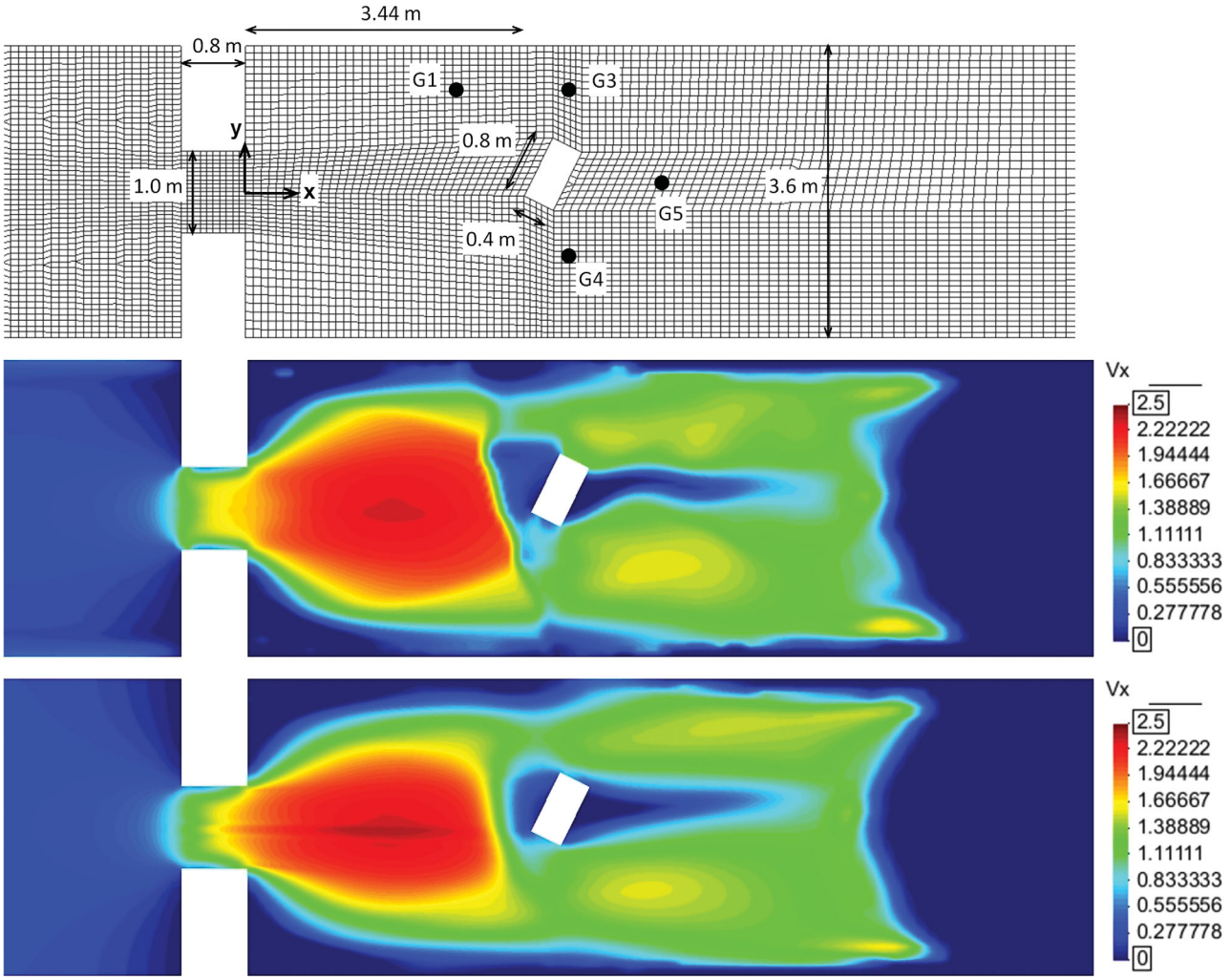

Figure 11. Test case T5. (top) Geometry and finite volume mesh used in the computations and velocity in the *x* direction 5 s after the gate opening, computed with the schemes of (middle) Roe and (bottom) DHD.

of Roe and it does not account properly for the celerity of the shock waves in the upwind discretization of the momentum and mass fluxes. In dam break and similar problems, the Roe scheme should be preferred to the DHD scheme, since it is a more robust and stable scheme in the presence of strong shock waves.

If we compare the water depth time series at the four gauge stations shown in Figure 11, the performance of the Roe and DHD schemes is very similar (Figure 12). The magnitude and the trend in the time evolution of the water depth is well captured by both schemes, but the local high-frequency fluctuations are not captured by any of them. This means that the structural error, which is due to the simplifications made in the shallow water equations (hydrostatic pressure distribution and uniform velocity profile in the vertical direction), is more relevant than the error due to the simplified discretization used in the DHD scheme.

3.6. CPU Time

In the previous sections, we have focused the analysis on the comparison of model results. Regarding the CPU time required by the different numerical implementations, in all the test cases the DHD scheme and the SI formulation outperform the scheme of Roe, since the number of operations per time step needed to compute the fluxes between adjacent cells is much lower with the former schemes. In addition, for the same flow conditions, the time step limitation given by the CFL condition is less restrictive in the SI model (equation (22)) than in the DHD scheme (equation (10)), although for the applications analyzed in this paper

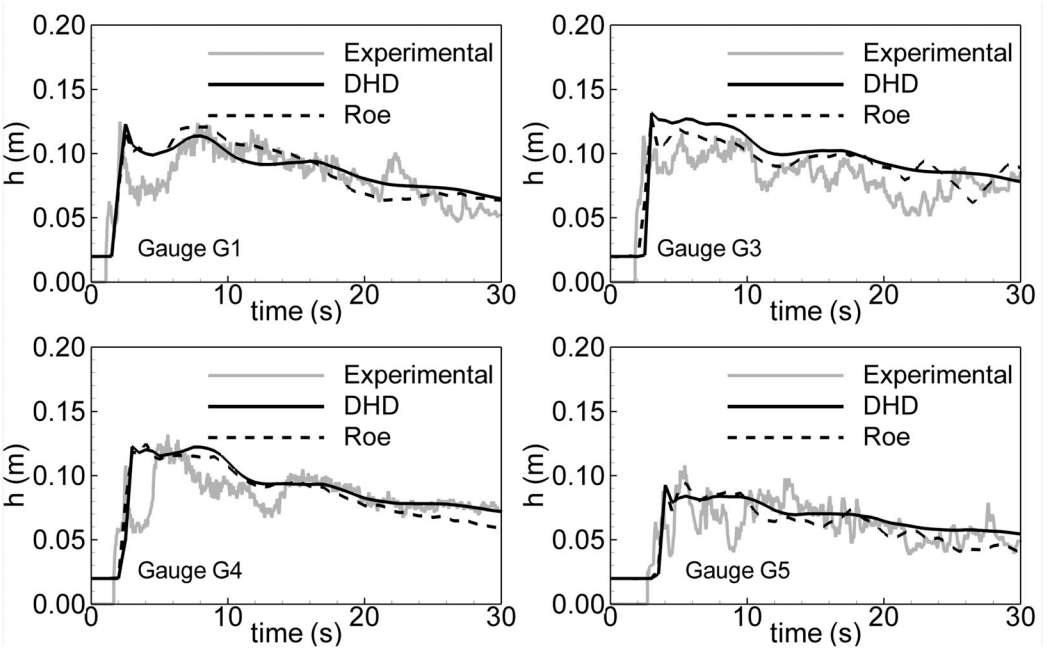

Figure 12. Test case T5. Time series of water depth computed and measured at the four water level gauges shown in Figure 11.

this theoretical advantage of the SI scheme is not strongly reflected in the CPU times required by each model (Table 1). The SI is nonetheless the fastest one in all the test cases. In the rural watersheds, where the results given by the DHD and SI schemes are very similar, the differences in CPU time between the SI and DHD implementations is of the order of 10%.

The ratio between the CPU times required by the DHD and Roe schemes is quite consistent for the different test cases, varying between 0.4 and 0.6 (Table 1). On the other hand, the ratio between the CPU time required by the DHD and DW models is strongly dependent on the test case. In the test case T1, the DW model runs two orders of magnitude slower than the DHD scheme. This is because in T1 the mesh resolution is very fine, the bed surface is smooth and the slope of the free surface is relatively low. According to equation (23), all these factors contribute to limit the maximum stable time step in the DW approximation. The magnitude of the CPU time differences is coherent with the results presented in *Bates et al*. [2010], who reported differences ranging from 1 to 3 orders of magnitude in the CPU times required by the SI and DW models. As it could be expected, the DW model is much faster when applied to the rural watersheds, where it outperforms the scheme of Roe, but not the DHD and SI. In coarser grids, the DW is expected to run even faster, although the dependence of the stable time step on the free surface slope remains a handicap for explicit implementations of this model.

The previous CPU times are related to the specific code structure in which the schemes were implemented, which is the same for all the formulations in order to test the schemes under the same implementation

Table 1. CPU Time Required for Each Test Case in a Intel Core i7 1.60 GHz[a]

	T1-R84	T1-R180	T1-R300	T2	T3	T4	T5
T_{DHD}	5	6	6	4	319	185	28
T_{Roe}	8	10	10	7	572	478	65
T_{SI}	4	6	6		284	170	
T_{DW}	245	343	547		510	190	
T_{DHD}/T_{Roe}	0.63	0.60	0.60	0.57	0.56	0.39	0.43
T_{DHD}/T_{SI}	1.25	1.00	1.00		1.12	1.09	
T_{DHD}/T_{DW}	0.02	0.02	0.01		0.63	0.97	

[a]As explained in the text, the DW and SI models were not used to compute the test cases T2 and T5, since these cases involve the computation of hydraulic jumps.

conditions and in the same grids. Stand alone implementations of each scheme, as well as structured grid discretizations, might be coded in a more efficient way. A further test of performance would be to compare optimized stand alone implementations of each scheme.

4. Conclusions

A simple finite volume scheme for solving the two-dimensional shallow water equations in hydrological applications involving overland flow and rainfall-runoff transformation in urban and rural basins has been presented. The scheme was validated against experimental laboratory and field data and compared to the classic finite volume scheme of Roe in five different test cases, which serve also as validation cases for the Iber software, the 2-D shallow water model used in all the simulations presented in this paper. In the test cases which do not involve generalized supercritical flow conditions the scheme was also compared to unstructured finite volume implementations of the SI and DW models. The test cases involve different kind of meshes, including unstructured, RTIN and block-structured grids, and cell sizes ranging from 4 cm to 30 m. The flow conditions, bed roughness, and terrain slope also vary widely from one case to another, implying that the relative magnitude of inertia, bed friction, and hydrostatic pressure also does.

The results presented here show that in typical overland flow applications the DHD scheme gives numerical solutions with similar accuracy and stability than the scheme of Roe, but with lower CPU time, having the additional advantage of its simplicity to code. Although the DHD scheme is better suited for surface runoff computations in urban catchments and small-scale rural basins, it can give acceptable results in the presence of strong unsteady shock waves, as shown in the dam break test case. Nonetheless, the scheme of Roe should be preferred in these kinds of applications due to its robustness and numerical stability. Regarding computational efficiency, in the test cases presented in this paper the CPU time required by the DHD scheme is in average 50% lower than that required by the scheme of Roe. Although this ratio might vary in other applications, it seems to be a good approximation since the five test cases which were used for comparison involve very different Froude numbers, mesh sizes, bed slopes, and surface roughness.

Compared to the SI formulation, the DHD scheme retains the advection terms in the momentum equations, which improves its performance in inertia dominated applications. Differences between these both schemes become negligible at the catchment scale, where the bed friction and topography are the dominant terms in the equations. In the test cases involving catchment scale applications, the SI model outperforms the DHD scheme regarding CPU requirements, with approximately 10% less of CPU time.

The comparison with the DW model confirmed the results obtained in previous studies, which point out the problems of purely diffusive approximations of the shallow water equations in the presence of depressions in the terrain or when used in combination with high-resolution meshes. The CPU times obtained with the DW model were consistently higher than those required by the DHD and SI schemes.

The previous CPU times refer to the specific implementations of the schemes used in this paper. A further test of performance would be to compare optimized *stand alone* implementations of each scheme and parallelization strategies.

The stability and capability of the DHD scheme to deal correctly with the different flow conditions involved in the test cases opens up the possibility of using the scheme for integrated hydrological-hydraulic inundation modeling in catchments of a few km^2, without the need of using two separate models for computing the rainfall-runoff transformation at the basin scale, and the flood wave propagation at the reach scale. This possibility should be explored in future studies.

Acknowledgments
The authors would like to thank Paul Bates for his helpful comments during the review process, which helped to improve the final version of this paper. We also acknowledge Manuel Alvarez Enjo for providing the rainfall and discharge field data used in the Maior River catchment test case. All the experimental data used in the test cases presented in this paper as well as the input data used in the numerical simulations are available upon request by mail to Luis Cea (luis.cea@udc.es). A version of the DHD solver has been implemented in the software Iber, which can be downloaded for free from (www.iberaula.com).

References

Audusse, E., and M. O. Bristeau (2003), Transport of pollutant in shallow water: A two time steps kinetic method, *Math. Modell. Numer. Anal.*, *37*(2), 389–416.

Bates, P. D., M. S. Horritt, and T. J. Fewtrell (2010), A simple inertial formulation of the shallow water equations for efficient two-dimensional flood inundation modelling, *J. Hydrol.*, *387*, 33–45.

Begnudelli, L., B. F. Sanders, and S. F. Bradford (2008), An adaptive Godunov-based model for flood simulation, *J. Hydraul. Eng.*, *134*(6), 714–725.

Benkhaldoun, F., I. Elmahi, and M. Seaid (2007), Well-balanced finite volume schemes for pollutant transport by shallow water equations on unstructured meshes, *J. Comput. Phys.*, *226*, 180–203.

Bermúdez, A., and M. E. Vázquez-Cendón (1994), Upwind methods for hyperbolic conservation laws with source terms, *Comput. Fluids*, *23*(8), 1049–1071.
Bermúdez, A., A. Dervieux, J. A. Desideri, and M. E. Vázquez-Cendón (1998), Upwind schemes for the two-dimensional shallow water equations with variable depth using unstructured meshes, *Comput. Methods Appl. Mech. Eng.*, *155*, 49–72.
Berthon, C., F. Marche, and R. Turpault (2011), An efficient scheme on wet/dry transitions for shallow water equations with friction, *Comput. Fluids*, *48*, 192–201.
Bladé, E., L. Cea, G. Corestein, E. Escolano, J. Puertas, M. E. Vázquez-Cendón, J. Dolz, and A. Coll (2014), Iber: Herramienta de simulación numérica del flujo en ríos, *Rev. Int. Métodos Numér. Cálc. Diseño Ing.*, *30*(1), 1–10.
Bradford, F., and B. F. Sanders (2002), Finite-volume model for shallow-water flooding of arbitrary topography, *J. Hydraul. Eng.*, *128*(3), 289–298.
Caleffi, V., A. Valiani, and A. Zanni (2003), Finite volume method for simulating extreme flood events in natural channels, *J. Hydraul. Res.*, *41*(2), 167–177.
Canestrelli, A., A. Siviglia, M. Dumbser, and E. F. Toro (2009), Well-balanced high-order centred schemes for non-conservative hyperbolic systems: Applications to shallow water equations with fixed and mobile bed, *Adv. Water Resour.*, *32*(6), 834–844.
Cea, L., and M. E. Vázquez-Cendón (2010), Unstructured finite volume discretisation of two-dimensional depth-averaged shallow water equations with porosity, *Int. J. Numer. Methods Fluids*, *63*(8), 903–930.
Cea, L., and M. E. Vázquez-Cendón (2012), Unstructured finite volume discretisation of bed friction and convective flux in solute transport models linked to the shallow water equations, *J. Comput. Phys.*, *231*, 3317–3339.
Cea, L., J. Puertas, and M. E. Vázquez-Cendón (2007), Depth-averaged modelling of turbulent shallow water flow with wet-dry fronts, *Arch. Comput. Methods Eng.*, *14*(3), 303–341.
Cea, L., M. Garrido, and J. Puertas (2010a), Experimental validation of two-dimensional depth-averaged models for forecasting rainfall-runoff from precipitation data in urban areas, *J. Hydrol.*, *382*, 88–102.
Cea, L., M. Garrido, J. Puertas, A. Jácome, H. del Río, and J. Suárez (2010b), Overland flow computations in urban and industrial catchments from direct precipitation data using a two-dimensional shallow water model, *Water Sci. Technol.*, *62*(9), 1998–2008.
Chertock, A., S. Cui, A. Kurganov, and T. Wu (2010), Well-balanced positivity preserving central-upwind scheme for the shallow water system with friction terms, *J. Hydrol.*, *382*, 88–102.
Chow, V. T., D. R. Maidment, and L. W. Mays (1988), *Applied Hydrology*, McGraw-Hill, N. Y.
Costabile, P., C. Costanzo, and F. Macchione (2012), Comparative analysis of overland flow models using finite volume schemes, *J. Hydroinformatics*, *14*(1), 122–135.
Courant, R., K. Friedrichs, and H. Lewy (1967), On the partial difference equations of mathematical physics, *IBM J. Res. Dev.*, *11*(2), 215–234.
de Almeida, G. A., and P. Bates (2013), Applicability of the local inertial approximation of the shallow water equations to flood modeling, *Water Resour. Res.*, *49*, 4833–4844, doi:10.1002/wrcr.20366.
de Almeida, G. A., P. Bates, J. E. Freer, and M. Souvignet (2012), Improving the stability of a simple formulation of the shallow water equations for 2-d flood modeling, *Water Resour. Res.*, *48*, W05528, doi:10.1029/2011WR011570.
Delestre, O., and F. Marche (2011), A numerical scheme for a viscous shallow water model with friction, *J. Sci. Comput.*, *48*, 41–51.
Duan, J. G. (2004), Simulation of flow and mass dispersion in meandering channels, *J. Hydraul. Eng.*, *130*(10), 964–976.
Engman, E. T. (1986), Roughness coefficients for routing surface runoff, *J. Irrig. Drain. Eng.*, *112*(1), 39–53.
Evans, W., D. Kirkpatrick, and G. Townsend (2001), Right-triangulated irregular networks, *Algorithmica*, *30*(2), 264–286.
Fraga, I., L. Cea, and J. Puertas (2013), Experimental study of the water depth and rainfall intensity effects on the bed roughness coefficient used in distributed urban drainage models, *J. Hydrol.*, *505*, 266–275.
Guinot, V., and S. Soares-Frazao (2006), Flux and source term discretization in two-dimensional shallow water models with porosity on unstructured grids, *Int. J. Numer. Methods Fluids*, *50*(3), 309–345.
Howes, D. A., A. D. Abrahams, and E. B. Pitman (2006), One- and two-dimensional modelling of overland flow in semiarid shrubland, Jornada basin, New Mexico, *Hydrol. Processes*, *20*, 1027–1046.
Hunter, N. M., M. S. Horritt, P. D. Bates, M. D. Wilson, and M. G. F. Werner (2005), An adaptive time step solution for raster-based storage cell modelling of floodplain inundation, *Adv. Water Resour.*, *28*, 975–991.
Hunter, N. M., P. D. Bates, M. S. Horritt, and M. D. Wilson (2007), Simple spatially-distributed models for predicting flood inundation: A review, *Geomorphology*, *90*, 208–225.
Hunter, N. M., et al. (2008), Benchmarking 2D hydraulic models for urban flooding, *Water Manage.*, *161*, 13–30.
Kim, D. H., Y. S. Cho, and H. J. Kim (2008), Well-balanced scheme between flux and source terms for computation of shallow-water equations over irregular bathymetry, *J. Eng. Mech.*, *134*(4), 277–290.
Kivva, S. L., and M. J. Zheleznyak (2005), Two-dimensional modeling of rainfall runoff and sediment transport in small catchments areas, *Int. J. Fluid Mech. Res.*, *32*(6), 703–716.
Leandro, J., A. Chen, and A. Schumann (2014), A 2d parallel diffusive wave model for floodplain inundation with variable time step (p-dwave), *J. Hydrol.*, *517*, 250–259.
LeVeque, R. J. (2002), *Finite Volume Methods for Hyperbolic Problems, Cambridge Texts in Applied Mathematics*, vol. 31, Cambridge Univ. Press, Cambridge, U. K.
Liang, D., L. Binliang, and R. A. Falconer (2007), Simulation of rapidly varying flow using an efficient tvdmaccormack scheme, *Int. J. Numer. Methods Fluids*, *53*, 811–823.
Liang, Q. (2010), Flood simulation using a well-balanced shallow flow model, *J. Hydraul. Eng.*, *136*(9), 669–675.
Liang, Q., and F. Marche (2009), Numerical resolution of well-balanced shallow water equations with complex source terms, *Adv. Water Resour.*, *32*(6), 873–884.
Marche, F., P. Bonneton, P. Fabrie, and N. Seguin (2007), Evaluation of well-balanced bore-capturing schemes for 2D wetting and drying processes, *Int. J. Numer. Methods Fluids*, *53*(5), 867–894.
Martinez-Gavara, A., and R. Donat (2011), A hybrid second order scheme for shallow water flows, *J. Sci. Comput.*, *48*(1–3), 241–257.
Muñoz-Carpena, R., J. E. Parsons, and J. W. Gilliam (1999), Modeling hydrology and sediment transport in vegetative filter strips, *J. Hydrol.*, *214*(1), 111–129.
Murillo, J., J. Burguete, and P. Garcia-Navarro (2008), Analysis of a second-order upwind method for the simulation of solute transport in 2D shallow water flow, *Int. J. Numer. Methods Fluids*, *56*, 661–686.
Nanía, L. S., M. Gómez, J. Dolz, P. Comas, and J. Pomares (2011), Experimental study of subcritical dividing flow in an equal-width, four-branch junction, *J. Hydraul. Eng.*, *137*(10), 1298–1305.
Neal, J. C., T. J. Fewtrell, P. D. Bates, and N. G. Wright (2010), A comparison of three parallelisation methods for 2D flood inundation models, *Environ. Modell. Software*, *25*(4), 398–411.

Ponce, V. (1990), Generalized diffusion wave equation with inertial effects, *Water Resour. Res.*, *26*(5), 1099–1101.
Ricchiuto, M., R. Abgrall, and H. Deconinck (2007), Application of conservative residual distribution schemes to the solution of the shallow water equations on unstructured meshes, *J. Comput. Phys.*, *222*, 287–331.
Ricchiuto, M., R. Abgrall, and H. Deconinck (2011), On the C-property and generalized C-property of residual distribution for the shallow water equations, *J. Sci. Comput.*, *48*, 304–318.
Roe, P. L. (1986), A basis for the upwind differencing of the two-dimensional unsteady Euler equations, *Numer. Methods Fluid Dyn.*, *2*, 55–80.
Sanders, B. F., J. E. Schubert, and H. A. Gallegos (2008), Integral formulation of shallow-water equations with anisotropic porosity for urban flood modeling, *J. Hydrol.*, *362*, 19–38.
Sanders, B. F., J. E. Schubert, and R. L. Detwiler (2010), Parbrezo: A parallel, unstructured grid, godunov-type, shallow-water code for high-resolution flood inundation modeling at the regional scale, *Adv. Water Resour.*, *33*(12), 1456–1467.
Sauvaget, P., E. David, and C. G. Soares (2000), Modelling tidal currents on the coast of Portugal, *Coastal Eng.*, *40*, 393–409.
Schubert, J. E., B. F. Sanders, M. J. Smith, and N. G. Wright (2008), Unstructured mesh generation and landcover-based resistance for hydrodynamic modeling of urban flooding, *Adv. Water Resour.*, *31*, 1603–1621.
Soares-Frazão, S., and Y. Zech (2007), Experimental study of dam-break flow against an isolated obstacle, *J. Hydraul. Res.*, *45*(suppl. 1), 27–36.
Toro, E. F. (2001), *Shock-Capturing Methods for Free-Surface Shallow Flows*, John Wiley, Chichester, U. K.
Toro, E. F. (2009), *Riemann Solvers and Numerical Methods for Fluid Dynamics: A Practical Introduction*, Springer, N. Y.
Valiani, A., V. Caleffi, and A. Zanni (2002), Case study: Malpasset dam-break simulation using a two-dimensional finite volume method, *J. Hydraul. Eng.*, *128*(5), 460–472.
Vázquez-Cendón, M. E. (1999), Improved treatment of source terms in upwind schemes for the shallow water equations in channels with irregular geometry, *J. Comput. Phys.*, *148*, 497–526.
Wang, Y., Q. Liang, G. Kesserwani, and J. W. Hall (2011), A 2d shallow flow model for practical dam-break simulations, *J. Hydraul. Res.*, *49*(3), 307–316.
Wilson, C. A. M. E., P. D. Bates, and J. M. Hervouet (2002), Comparison of turbulence models for stage-discharge rating curve prediction in reach-scale compound channel flows using two-dimensional finite element methods, *J. Hydrol.*, *257*, 42–58.
Wu, W. (2004), Depth-averaged two-dimensional numerical modeling of unsteady flow and nonuniform sediment transport in open channels, *J. Hydraul. Eng.*, *130*(10), 1013–1024.
Yoon, T. H. (2004), Finite volume model for two-dimensional shallow water flows on unstructured grids, *J. Hydraul. Eng.*, *130*(7), 678–688.